An Experimental Study of Methane Hydrate Growth and Dissociation in Porous Media

Master Thesis in Reservoir Physics

By

Erik Rasmussen Vadla

Department of Physics and Technology
University of Bergen

June 2015

Abstract

Natural gas hydrate (NGH) is a solid phase consisting of water and natural gas. NGH represents a justified vast global energy resource, and is widespread in on-shore artic and sub-seafloor environments. Due to the worlds increasing demand for energy, and pressing environmental issues, methane (CH_4) production from NGH represent a favorable option towards more energy security and sustainability.

This thesis presents a series of experiments conducted on sandstone core samples. The main focus of the experiments was to gather data from hydrate formation and different gas productions schemes in porous media. The results from the experiment contribute to an in-house database which is used to develop numerical models for hydrate systems. Bentheimer sandstone was used in all the core scale experiments. All the cores were saturated with 3.5wt% NaCl prior to the experiments and had fairly high initial water saturation in the range of 0.57-070.

CH_4 hydrate formation was conducted in 15 different Bentheimer sandstone cores. The core temperature during formation was in the range of 0-4°C, depending on the experiment. Final hydrate saturations ranged from 0.40-0.64 which is consistent with previous experiments. The impact on growth patterns due to salinity variations was inspected by comparison with previous experiments with 0.1wt% NaCl. Salt lowers the water activity and shifts the hydrate stability line towards lower temperatures. A clear trend showed higher initial growth rate in the low salinity hydrate formations. The salinity of the formation water showed no clear correlation with the final hydrate saturation in the concentration range investigated.

Pressure induced dissociation was conducted by 0.7bar pressure steps on 10 Bentheimer cores. There was an expected correlation between core temperature and dissociation pressure. The amount of gas released (2-12ml) on each pressure step was lower than expected and 8-12 pressure steps were needed to produce all the methane. Similar experiments previously conducted reached a full recovery after three pressure steps (0.7 bar each), but these had a lower salt concentration in the formation water (0.1 wt%). The large amount of pressure steps needed for full recovery is believed to be caused by a decrease in salinity as water molecules are released during dissociation, thus shifting the hydrate phase boundary to lower pressures.

Even more pressure steps were needed to fully dissociate the sandstone core containing a mixed hydrate of CO_2 and CH_4. 14 small (0.7bar) and 1 large (11.8bar) pressure steps was executed to fully dissociate the hydrate. This was due to the variation in melting pressure depending on the molar fractions of the two components inhabiting the hydrate. Pure CO_2 hydrate and pure CH_4 hydrate has an estimated melting pressure of 24.35 and 45.03 bars in bulk at 4°C and 3.5wt% NaCl, respectively. Dissociation was first observed at 42.9 bars in the experiment.

Methane production through CO_2/CH_4 resulted in an estimated CH_4 recovery of 0.25 from hydrate. Due to high excess water saturation (0.31) after hydrate formation the N_2 was co- injected with CO_2 with the ratio 60(N_2)/40(CO_2) to prevent CO_2 from initiating hydrate formation with the excess water. The applied production scheme was a flush-sequence where the fluid mix was injected in several intervals ranging from 2-8.8 hours. A Gas Chromatograph was used together with a mass flow meter to determine to composition and amounts of the produced gas.

Acknowledgements

First of all I would like to thank my supervisor Associate Professor Geir Ersland for providing such an interesting subject for my thesis. Thank you for all the guidance with the accompanying coffee and for your good spirit and wisdom.

Thanks to Professor Arne Graue and Associate Professor Martin Fernø for facilitating my work here at IFT.

Thanks to Lars Petter Hauge for being more than helpful during the last year, a lot of time was saved due to your good advice and guidance, thank you.

Thanks to my lab-partner Stian Almenningen. It has been a pleasure working with you. Your good spirit and excellent work ethic is an inspiration. Your assistance during the last period has contributed a lot to this thesis.

I will also like to thank my fellow students creating a friendly ambiance in the office and for the numerous conversations and discussions on and off topic.

At the end I would like to thank my soon-to-be cohabitant Josef Flatlandsmo for creating a lot of laughter and joy as well as providing insight to hydrate related topics. Thank you for all the great lunches and the other break related activities.

Table of Contents

Introduction

As the global climate changes are getting more apparent, the world's energy focus has shifted towards greener and more sustainable forms of energy. Even though the technology within wind, solar, wave and geothermal energy has improved, it does not cover the energy need of the entire planet, yet. Recent estimates suggest that more than 80% of the world's energy supply comes from fossil fuels. Coal, oil and natural gas are examples of fossil fuels. Natural gas has a lower carbon footprint than oil and coal (Energy, 2014). This makes natural gas favorable in a transition period towards a more sustainable future. Developing efficient and commercially viable production schemes that favors the environment is crucial in order to reduce the large amount of greenhouse gases currently emitted.

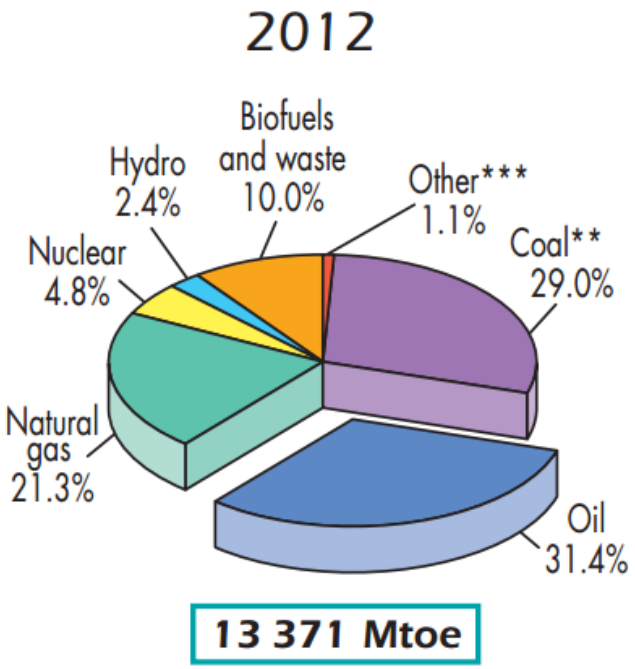

Fig 0.1 – Overview of the world's energy supply in 2012. The total supply equals 13371 Mtoe (toe= tonne oil equivalent =10^7 kcal). **in this graph, peat and oil shale are aggregated with coal. ***includes geothermal, solar, wind, heat, etc (International Energy Agency, 2014).

Most of the natural gas is produced from conventional oil and gas reservoirs, and from shale gas. Another potential gas source is natural gas hydrates (NGH), which is the focus in this thesis. There are different estimates trying to determine the resource extent and the production feasibility of methane from NGH. The resource potential has been estimated in the range of 10^{15} to 10^{17} m^3 of methane at standard conditions (Kvenvolden, 1988) (Klauda & Sandler, 2005). To identify how much of the resources that were actually producible, Bosewell and Collett estimated the production potential of the different geological features the natural gas hydrates inhabits *(Fig 0.2).*

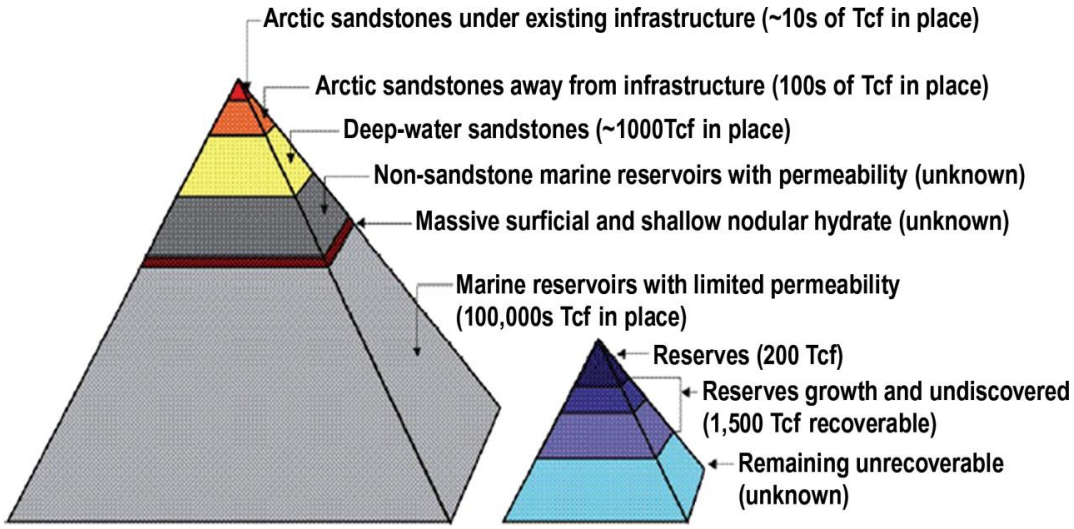

Fig 0.2 - A resource pyramid showing quantities of methane in different geological formations. The small pyramid to the right represents all non-hydrate gas resources (Bosewell & Collett, 2006).

Many countries are now assessing their hydrate resource potentials. India for instance has done extensive seismic surveying on their continental shelf that shows great promise. The estimated hydrate resources are 1,894 trillion m^3, which is 1700 times more than the conventional gas resources estimates in India (Jha & Bansal, 2012). Locating and identifying the resources is only one part of the process, in order to exploit the energy in the hydrate, the methane must be extracted. The most environmental friendly production scheme proposed, sequestrates CO_2 while producing methane. Other production schemes involve depressurization, thermal stimulation and chemical inhibitors.

This thesis is based on experimental work and the main objective is to provide statistical data to understand the nature of hydrate-bearing sediments and add to an in-house database created for this purpose. The majority of the experiments are conducted using sandstone core samples with high initial water saturation. Hydrate formation, pressure induced dissociation and methane production through CO_2-sequestration will be investigated through these experiments. Gas hydrate systems are complex, and statistical data is important in order to develop accurate models that can predict such systems.

Chapter 1 - Fundamentals

Natural gas hydrates (NGH) is a solid consisting of water and natural gas. NGH has a crystal structure, and its appearance and physical properties much in resembles ice. A major difference is that NGH is flammable, and are often referred to as “Burning ice”.

This chapter will provide information about the role of both water and gas in the hydrate, different hydrate structures, hydrate formation, hydrate deposits and different production techniques. Production schemes used in the experimental work were pressure depletion and CO_2 sequestration, so these two will be emphasized.

1.1 The water molecule

Water is a substance with a lot of interesting properties. Some of these properties are due to the hydrogen bonding between the water molecules. The two hydrogen atoms and the oxygen atom is arranged non-linear with 104,45°angle between the two covalent bonds and makes it easy for the water molecules to create hydrogen bonds with each other (Stillinger, 1980).

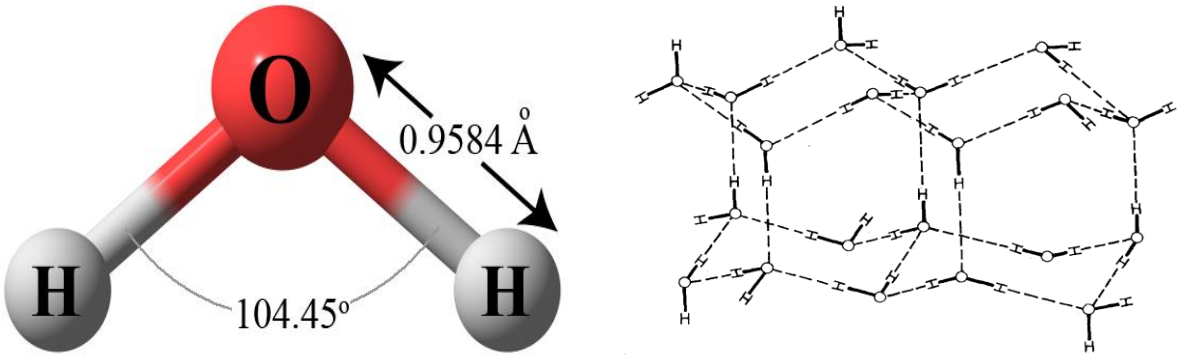

Fig 1.1.1 – To the right we see the water molecule and the atom arrangement (Ch'ng, u.d.). The left figure illustrates the hexagonal structure of ice, where the dashed lines represent the intermolecular hydrogen bonds and the solid lines represent the covalent bonds between hydrogen and oxygen (Stillinger, 1980).

The hydrogen bonds are strong compared to the weak van der Waals interactions, the bond strengths are 5 kcal/mole and 0,3 kcal/mole respectively, and these are inter molecular bonds. The covalent bonding is an intra-molecular bond and has the strength of 100 kcal/mole (Stillinger, 1980). Water has a specific heat capacity of 4,184 kJ/(kg *°C) (Chang, 2006) and is a good heat conductor. 34% of the volume in regular ice is occupied by water molecules while 37% of the volume in liquid water. This leads to a 10% volume expansion as water freezes (Sloan & Koh, 2007). Ice has a hexagonal structure, illustrated in *Fig1.1.1*, where the hydrogen bonds keep the structure together.

1.2 Properties of CH_4 and CO_2

Gas solubility in water is pressure and temperature dependent. The solubility of CH_4 and CO_2 are both increasing with increasing pressure and decreasing temperature. The solubility of CO_2 in water is about 13 times larger than CH_4 in water when hydrates are present in the system, 0.83 and 0.063mol/kg respectively (Jung, et al., 2010). Another important factor is that the liquid-vapor (L-V) of CO_2 is highly affected by the presence of methane. The phase boundary between liquid and gas for pure CO_2 is at 38.6 and at 60.0 bars for temperatures of 4 and 22°C respectively (Wischnewski, u.d.). The two temperatures (4 and 22°C) are the most used operation temperatures in the experimental work in this thesis. A mix of CO_2 (90%) and CH_4 (10%) needs 20bar more to condense than pure CO_2 (Jung, et al., 2010).

The diffusivities of CO_2 and CH_4 in water are fairly similar (~10^{-9} m^2/s), and it is the controlling factor for the phase distribution in a long term perspective. The diffusivity of water in liquid CO_2 on the other hand, has a value up to 2 orders of magnitude larger then CO_2 and CH_4 in water. Combined with a relatively high solubility (0.050 mol/kg) of water in liquid CO_2, make liquid CO_2 an effective water-drying fluid agent (Jung, et al., 2010).

1.3 Hydrate Structures

Structure 1 (sI), Structure 2 (sII) and structure H (sH) are the three known hydrate structures. Each structure has a distinct set of water molecule cages that makes a unit cell. A common nomenclature description of these cages is n_i^{mi}, where n_i is the number of edges in face type "i" and m_i is the number of faces with n_i edges (Sloan, 1998).

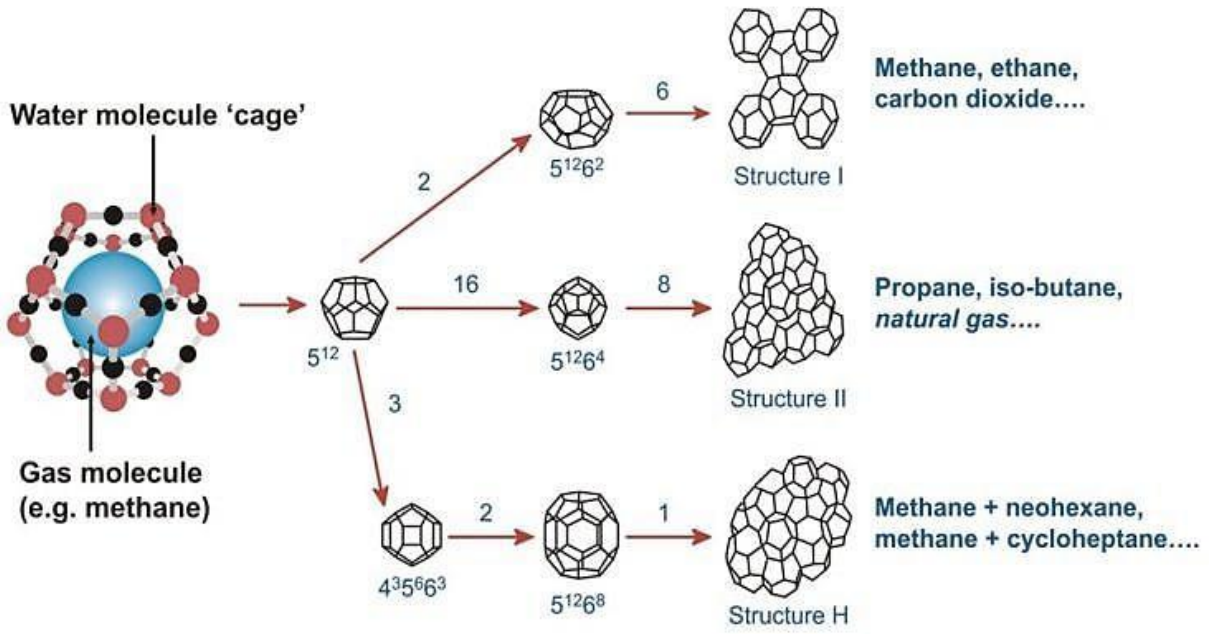

Figure 1.3. - Different hydrate structures and their building blocks **(HWU, 2013)**.

Table 1.3. – Overview of the different cages and unit cell ratios making up the hydrate structures **(Sloan, 1998)**

Structure	sI		sII		sH		
Cavity	Small	Large	Small	Large	Small	Medium	Large
Description	5^{12}	$5^{12}6^2$	5^{12}	$5^{12}6^4$	5^{12}	$2*4^35^66^3$	$5^{12}6^8$
Number of cavities/unit cell	2	6	16	8	3	2	1
Average cavity radius[Å]	3,95	4,33	3,91	4,73	3,91	4,06	5,71
Water molecules/unit cell	46		136		36		

SI and sII is the two structures found in nature, while sH have only been proven in the laboratory. sI and sII will be the main focus in this thesis. *Figure 1.3.* shows that sI and sII are build up differently. In sI, the 5^{12} cavities are linked together by their vertices, while sII illustrates face-sharing of the 5^{12} (Sloan, 1998).

1.4 The guest molecule

Together with the water molecule, the guest makes up the gas hydrate. The properties of the hydrate mainly depend on the polarity and the size of the guest molecule. A thumb rule is that the size ratio between the cavity and the guest molecule should range from 0.76 to 1. If the ratio is bigger than 1, the guest does not fit, and if it is smaller, the molecular attractive forces cannot contribute to cavity stability. (Sloan, 1998). Experiments on hydrates in bulk have shown that smaller molecules, like N_2, can have multiple molecules within one cavity (Park, et al., 2008). Some of the experiments in this thesis are conducted with systems containing N_2, CH_4 and CO_2 simultaneously. This makes it difficult to determine the hydrate composition.

Table 1.4 – A list of the three guest molecules and their size ratios (Sloan, 1998).

		Molecule diameter/cavity diameter (size ratio)			
		Structure I		Structure II	
Molecule	Guest diameter [Å]	5^{12}	$5^{12}6^2$	5^{12}	$5^{12}6^4$
N_2	4,1	0,804	0,700	0,817	0,616
CH_4	4,36	0,855	0,744	0,868	0,655
CO_2	5,12	1,00	0,834	1,02	0,769

1.4.1 Cyclopentane

Cyclopentane can also be used as a hydrate former. The major difference between the cyclopentane hydrate and hydrates including the substances listed in *table 1.4.1* is the phase diagram. Cyclopentane hydrate is stable at atmospheric pressures for temperatures lower than 7°C (Karanjkar, et al., 2011), which makes hydrate formation possible without the need of high pressure pumps and pressure cells. Both methane and cyclopentane have low water solubility therefore hydrate formation is likely to occur at the interface between the hydrate former and water. Other properties such as boiling point of 50°C and relatively cheap makes cyclopentane an attractive as a hydrate research tool (Dirdal, et al., 2012).

1.5 Hydrate formation and kinetics

To locate producible NGH deposits it is important to know under what conditions they form. This makes it possible narrow down the search. The formation conditions depend on the guest molecule, the composition of both the formation water and the formation. Below are some general requirements for the occurrence of hydrate formation:

- Favorable temperature and pressure conditions
- Sufficient host and guest molecules
- The change in Gibbs free energy (ΔG) has to be negative for the reaction

The pressure/temperature stability region is different for CO_2 hydrate compared to CH_4 hydrate, as shown in Fig 1.5.1. For temperatures below approximately 10°C, the CO_2 hydrate is more stable than CH_4 – hydrate. The experiments in this thesis are conducted at temperatures in the range of 0 - 4°C and CO_2 will be referred to as the more stable guest molecule. The stability curves in *Fig 1.5.1* are calculated through the CSMgem software. Pure CO_2 hydrate and pure CH_4 hydrate has a calculated formation pressure of 24.35 and 45.03 bars at 4°C and 3.5wt% NaCl, respectively. The mathematical model in the software is based on bulk hydrates. The experiments in this thesis is done with hydrates in a porous media, so the quantitate values from the software does not coincide with the expected experimental values. Hydrate formation in porous media involves extra parameters that complicate the system. The matrix and the pore network leads to adsorbed phases, impurities in the formation water such as NaCl also affects the hydrate stability zone. The combination of all the extra parameters makes it more difficult to predict how the system will evolve in terms of hydrate saturation and phase distribution. CSMgem is a useful tool to investigate qualitative properties of different hydrate mixtures.

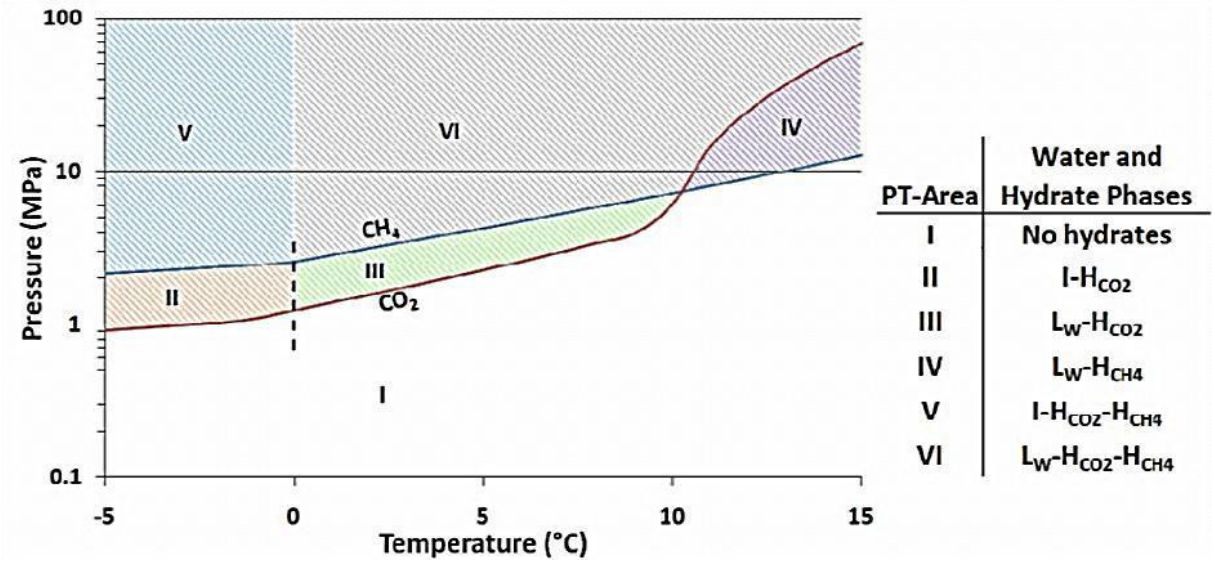

Fig 1.5.1 – Stability curves for CH_4 and CO_2 hydrate (Husebø, 2008). Retrieved from CSMgem.

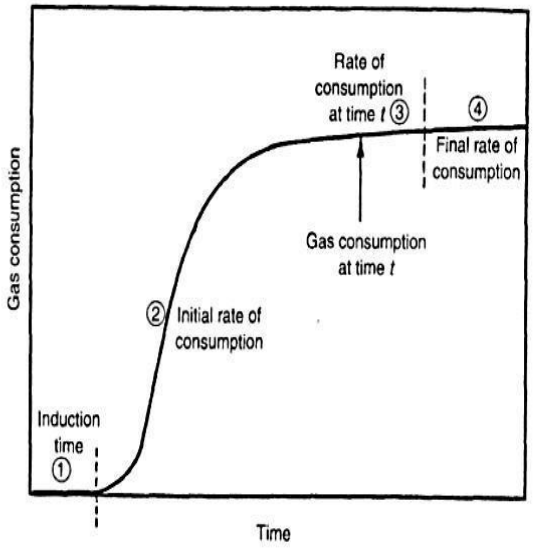

Fig 1.5.2 – A scheme over gas consumption in the different hydrate formation stages. This system is being held at constant temperature and pressure. The system has excess gas, and has a limited amount of water (Sloan & Koh, 2007)**.**

Nucleation time is the time needed to overcome the balance between penalty and gain during formation the first hydrate units. Where the gain is the negative change in Gibbs free energy related to the phase transition and the penalty is the positive contribution to the total Gibbs free energy because of the decrease in entropy (Kvamme, 2014). There are two different kinds of nucleation, homogeneous (HON) and heterogeneous (HEN) nucleation. HEN is crystallization at the interface of different fluids, while HON occurs in bulk in the absence of impurities (Sloan & Koh, 2007).

Induction time, marked as 1 on *Fig 1.5.2*, is the time it takes for onset of massive growth from the point the system enters hydrate stable conditions. During this period, the hydrate is in a metastable zone, were both formation and dissociation can occur. It is found that the induction time is stochastic and not deterministic, during the induction time the probability of the system state is spread over a range of values. High driving forces leads to a less stochastic system, with a more narrow range of values. Low driving forces makes the system more stochastic and less predictable (Sloan & Koh, 2007). If there is sufficient host and guest molecules, and beneficial mass and heat transport the massive growth can take place. In the period of massive growth, the hydrate is stable, and will not dissociate if the system is being kept at the present conditions. As the hydrates are formed, the mass transport is limited by the solid hydrate phase, and the rate of formation will decrease.

There are many routes to hydrate formation, and each route results in hydrates with different Gibbs free energies (Kvamme, 2014). The routes depend on which faces are involved in the formation. The routes that are most relevant for this thesis are:

- H_2O (l) + CH_4 (g) = H_{CH41} (1)
- H_2O (ad) + CH_4 (g) = H_{CH42} (2)
- H_2O (l) + CO_2 (l) = H_{CO21} (3)

Where *l*, *g* and *ad* are liquid, gas and adsorbed face respectively. And H_{CH41}, H_{CH42} and H_{CO21} are different hydrates formed. Due low solubility of methane in water (0.0788-0.1645 mol/kg for brine at

3.5 weight % NaCl (Duan, et al., 1992)), the hydrate tend to form at the gas/liquid interface and not between dissolved gas and water. A reason for this is the limited mass transport of dissolved methane molecules in water. In water wet porous media the water will stick to the pore walls and gas bubbles are mainly found in the larger pores, and will occupy the center of these, therefor there is also more hydrate growth in larger pores (Kleinberg, et al., 2003).

Englezos et al. (1987) suggested a model for hydrate growth:

$$\left(\frac{dn_i}{dt}\right)p = K^* A_p \left(f_i^b - f_i^{eq}\right)$$

$$\frac{1}{K^*} = \frac{1}{K_r} + \frac{1}{K_d}$$

Where:

n_i = Number of gas molecules consumed in the hydrate, t= time , A_p = Surface area,

f_i^b= fugacity of component i in the bulk liquid

f_i^{eq}= equilibrium fugacity of component i in the liquid at the hydrate interface

K*= Hydrate formation growth rate constant

K_r = reaction rate constant, K_d = mass transfer coefficient through the film around the particle

This model shows that the hydrate growth depends on the surface area of the fluid/hydrate interface and the fugacity difference of the hydrate former in the bulk and at the hydrate interface. More recent studies suggest that mass and heat transport has a bigger impact on hydrate growth than the intrinsic kinetics (Sloan & Koh, 2007).

1.5.1 The "memory effect"

The "memory effect" states that hydrate forms more easily from gas and water obtained from melted hydrate, than from gas and water without hydrate history. This effect is apparent when hydrates are melted within a moderate temperature range. If the post-hydrate gas/water system is heated sufficiently above the hydrate stability zone, or the system is left for a sufficient amount of time, the "memory effect" will be destroyed. The most common hypotheses are: (1) Hydrate structures left in solution after hydrate dissociation. (2) A persistent concentration of dissolved gas that remains in solution after dissociation. Decreased induction times have been observed in experiments when reforming hydrate, due to the "memory effect" (Sloan & Koh, 2007).

1.6 The origin of gas hydrates

Accumulation of NGH is found worldwide in places where the pressure is high (>40bar) and the temperature is low (<12°C). Around 99% of the NGH is found in oceanic sediments and the rest in onshore artic environments (Ruppel, 2011). Water and methane also needs to be present to form methane hydrates. The methane is either thermogenic or biogenic. Thermogenic methane is formed from thermal cracking of organic material, such as kerogen. The temperatures are too high (60-120°C) for the hydrates to grow where the gas is formed. The gas migrates through the porous media until the conditions are within the hydrate stable zone, and water is present. Biogenic gas originates

from anaerobe bacterial decomposition of organic matter. This process can take place under hydrate stable conditions thus the gas does not have to migrate (Hester & Brewer, 2009).

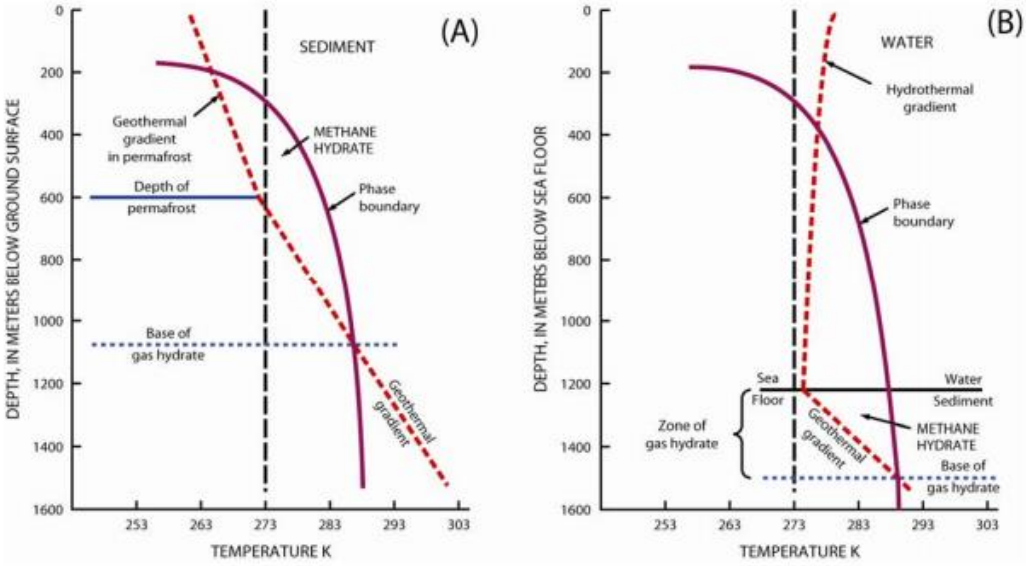

Fig 1.6. - Schematics of the geothermal gradient and the methane hydrate phase boundary for onshore artic permafrost (A) and marine environment (B).

1.7 Classification of hydrate bearing reservoirs

Even though hydrate is only found in marine and artic environments there are different hydrate accumulations within the two areas. These are classified by the hydrate concentration and by possible fluids present. NGH accumulations are divided into three main classes (Moridis, et al., 2010):

1. A hydrate bearing layer with underlying two phase fluid zone with mobile gas and water.
2. A hydrate layer with an underlying water zone.
3. A Hydrate layer without any underlying fluid zone.
4. Scattered low saturation hydrates without any free fluid phase present.

In (1) the conditions on the hydrate/fluid boundary coincide with the hydrate stability line. This makes it the most beneficial hydrate reservoir, with respect of gas production, because the least amount of energy is needed to dissociate the hydrate. (2) and (3) might be producible, but because of the absence of a gas phase the conditions could be far within the hydrate stable zone. (4) shows little promise of commercial production due to the dispersed and low hydrate saturation (<10%) (Moridis, et al., 2010). To get a high saturated hydrate layer there needs to be a geologic trap to accumulate the natural gas as it is created.

1.8 Hydrate Dissociation and production schemes

"Hydrate dissociation is an endothermic process in which heat must be supplied externally to break the hydrogen bonds between water molecules and the van der Waals interaction forces between the guests and water molecules of the hydrate lattice to decompose the hydrate to water and gas." (Sloan & Koh, 2007). To dissociate the hydrate, the pressure and temperature conditions have to move out of the hydrate-stable zone or there has to a shift in the hydrate stability line due to hydrate inhibitors. Here is three proposed ways of producing methane gas by dissociating the hydrate:

1. Thermal stimulation
2. Pressure induced dissociation
3. Thermodynamic inhibitor injection

All of these three are potential gas production techniques, but this thesis will emphasize depressurization. Many agree that this method shows the most promise for commercial production of methane from NGH. The sketch in the middle in *Fig 1.8* shows a depressurization scheme where there is a hydrate layer overlaying a layer of free gas (class 1). A well is drilled through the hydrate layer, and the free gas is produced. As the pressure is reduced in the reservoir, the hydrate is dissociated. The Russian Messoyakha Gas Field is supposedly produced in this manner. It was first thought that this field only contained free gas, but as the field was produced, the depressurizing slope flattened, which indicate an overlaying hydrate layer (Grover, et al., 2008). A report states that due to the endothermic nature of hydrate dissociation, freezing of the formation water and hydrate re-formation occurred during production of the Messoyakha field. Antifreeze solutions were injected into the reservoir to solve the issue (Grace, et al., 2008). Another problem related to production schemes involving hydrate dissociation is water and sand production. In unconsolidated sediments, hydrates may contribute to the geomechanical stability of the formation, dissociation the hydrates can lead to a collapse of the formation.

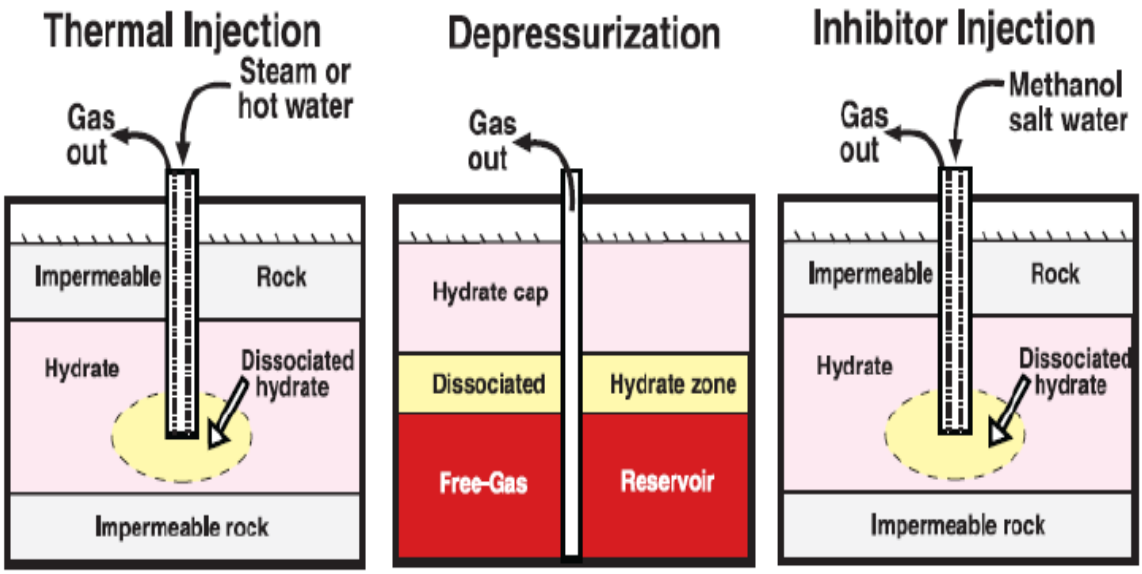

Fig 1.8 – Illustration of three different production mechanisms (Collett, 2002).

1.8.1 CO_2/CH_4 exchange

This is a production scheme where CO_2 is sequestrated to produce methane gas. By exposing the methane hydrate with CO_2, the methane hydrate will be converted to CO_2 hydrate (Graue, et al., 2008). *Fig 1.5.1* shows that CO_2 hydrate is stable at lower pressures than the methane hydrate at temperatures lower than 10°C. When the CO_2/ CH_4-exchange process takes place, the potential energy of the system decreases and energy is released in form of heat (Birkedal, 2013).The CO_2 molecule is bigger than the methane molecule, and as *Table 1.4.1* suggest, the CO_2 molecule has a favorable size relative to the $5^{12}6^2$ cavity in structure I. Experiments done on hydrates in bulk by Park et al. (2008) was done by exposing methane hydrate to a mix of N_2 and CO_2. They found that the N_2 would compete with CH_4 for the small cages while CO_2 would occupy the big cavities. SII and sH that was exposed to the gas mix would convert to sI. Recoveries between 64-95% were observed in these bulk experiments (Park, et al., 2008).

The three production mechanisms mentioned earlier dissociates the hydrate, while CO_2-sequestration maintains the integrity of the hydrate formation. This is a major advantage in areas where gas hydrates cements unconsolidated sediments due to the reduced risk of formation collapse during methane production. Another advantage with this production scheme is the CO_2 storage potential and records show more than 50% of injected CO_2 is trapped on field scale (Schoderbek, et al., 2012). A challenge with CO_2 sequestration is to prevent hydrate plugging due to CO_2 hydrate formation in the free water face in the reservoir which leads to reduced permeability. Co-injection of N_2 and CO_2 has been used with success in a field trial (Schoderbek, et al., 2012) to avoid plugging and maintain injectivity. Another challenge is to get a big enough contact area between the CO_2 and the CH_4 hydrate to get a satisfying CH_4 production rate.

1.9 Measurement techniques and imaging

Measurements and imaging done on the cores during the experiments is important to get an indication of the processes taking place. A high pressure pump is used in all the experiments done on the hydrate core lab. The pump log provides useful information about volume and pressure changes. By interpreting these data logs it is in many cases possible to identify hydrate formation, dissociation, temperature changes and identify leakage. Additional tools such as resistivity measurements and MRI makes it easier to determine the state of the system.

1.9.1 Resistivity measurements

Resistivity logging is widely used in conventional oil and gas exploration. This technique can also be applied when monitoring hydrate creation and dissociation. By sending a current through an area of interest, the resistivity of this area can be obtained. The Archie relations below are not used directly in this thesis, but they show a correlation between the resistivity and important reservoir parameters.

Archie's relations:

1. $F = \frac{R_o}{R_w} = a\varphi^{-m}$

The first relation describes the formation factor, F. *Ro* is the resistivity of a porous medium 100% saturated with brine and *Rw* is the resistivity of the brine itself. The ratio between the two resistivities, describes how the formation affect the resistivity. *a* is a function of tortuosity and the

pore size distribution, ϕ is the porosity and m is the cementation factor and depends on the consolidation of the matrix. (Lien, 2004)

2. $I = \frac{R_t}{R_o} = bS_w^{-n}\mathrm{er}$

The second relation describes how the fluid in the system affects the resistivity. R_t is the resistivity of the reservoir containing the actual fluid saturations, b is a tortuosity function, S_w is the water saturation and n is the saturation index. (Lien, 2004)

When hydrates are formed in a porous media, there are two major factors that affect the resistivity of the system. (1) Because hydrates have a very high resistivity, the tortuosity of the system increases, and as a result; the resistivity increases. (2) The density of salt increases as hydrates are formed, and the resistivity decreases. Experiments done by Ren et al. (2010) on sandpacks saturated with brine (3.5% NaCl) , shows that on hydrate saturations <20% the salt increase is dominating, and the total resistivity is reduced. With hydrate saturations>20% the tortuosity increase is the dominating factor, and the total resistivity increases (Ren, et al., 2010).

1.9.2 Magnetic Resonance Imaging

A useful tool in hydrate research is magnetic resonance imaging (MRI). This is an imaging technique that uses magnetic fields to study the precession of nuclear spins. A substance with a dipole moment (μ) unequal to zero gets magnetized (M_0) when placed in a static magnetic field (B_0). The Larmor-frequency is the precession frequency given by $w_0=yB_0$, where y is the gyromagnetic ratio of the particle in question (Lien, 2004). Magnetic pulses with high frequency, also called radio frequent pulses, temporary change the magnetization vector of the precessing particles. When the magnetic pulse is gone, the system returns to its equilibrium state. The time it takes to reach this equilibrium is called relaxation time.

T_1 is the characteristic time for the spin-lattice relaxation which is the transition from high to low magnetic energy (Ersland, 2008). The inversion-recovery method is frequently used to find T_1. A 180° pulse excites the system and the magnetic vector (**M**) becomes negative. After a time τ, a 90° makes the **M** value readable for the apparatus. This process is repeated for different values for τ (Lien, 2004).

T_2 is the characteristic time for the spin-spin relaxation. This relaxation process is due to interaction and energy loss between the particles, not interaction with the surroundings as in the spin – lattice relaxation. One way to measure T_2 is to use a method called spin-echo sequence. This sequence consists of a 90° pulse followed by a series of 180° pulses (Lien, 2004).

Chapter 2 - Literary survey

This chapter contains results from earlier work which is sentral for this thesis. The results in question are related to methane production from both pressure induced hydrate dissociation and CO_2/CH_4 exchange.

2.1 Field scale production tests

Field scale production tests are important in order to identify challenges which may be absent during laboratory tests. The most recent test conducted was the offshore pressure depletion test in the Nankai Trough, Japan. The two other tests were conducted in artic onshore environment.

2.1.1 Ignik Sikumi

In 2011 in the Alaskan North slope the first CO_2/CH_4-exchange production trial took place. The field trial was done by the University of Bergen together with ConocoPhilips. A single well was drilled down to 2600ft, and it would work as both injection and production well. Four hydrate bearing layers were encountered and the one called "Upper C" showed the most promise due to the high interpreted hydrate saturation, homogeneous character, and temperature/pressure conditions close to the ones tested in the laboratory (Schoderbek, et al., 2012).

During a two week period 210 mscf of a 23% CO_2 + 77%N_2 (mol %) mix was injected into Upper C. The added N_2 was to reduce the loss of injectivity due to secondary hydrate formation from the free water in the pore space. Five weeks with production, resulted in nearly 1000mscf of gas at 175,000 scf/day and more than half of the 48 mscf CO_2 injected remained in the formation (Schoderbek, et al., 2012) .This field trial showed that methane production from CO_2-sequestration is possible, and has a commercial potential.

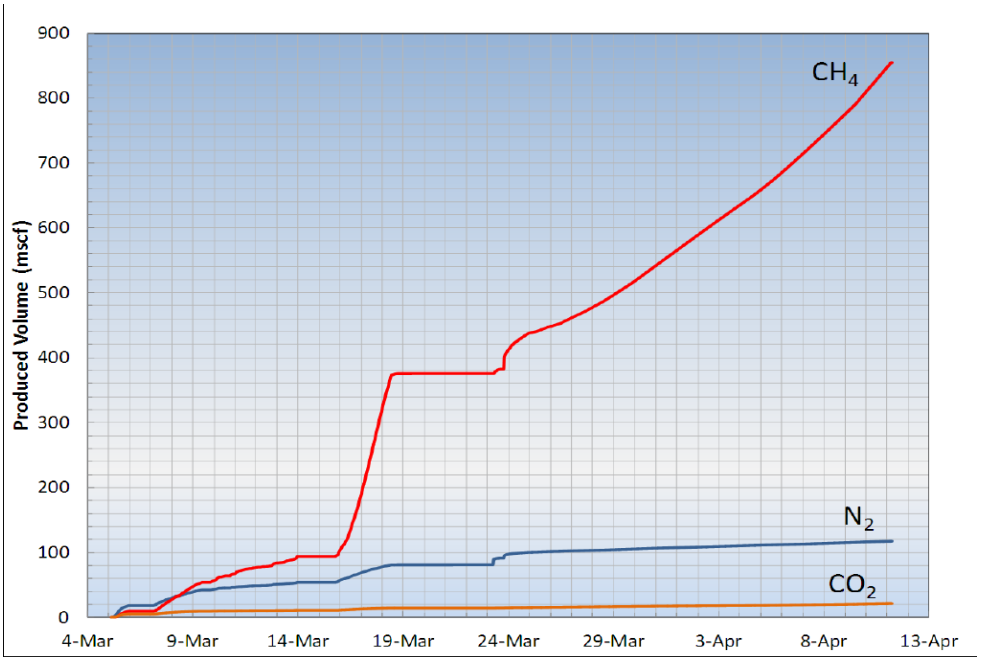

Fig 2.1.1 – Gas production from Ignik Sikumi field trial (Schoderbek, et al., 2012).

2.1.2 Nankai Trough

The First offshore methane hydrate production test was executed in 2013 in the eastern part of the Nankai Trough in Japan. The field was produced by depressurization and the test lasted 6 days. 120,000 m^3 of methane was produced (JOGMEC, 2014). The gas production rate was higher than the numerical models predicted. On day 6 of the test, the water cut increased followed by a strong sand flow, and production was shut down. Long-term behavior of the gas production was not obtained because of the early shut down. (Yamamoto, et al., 2014).

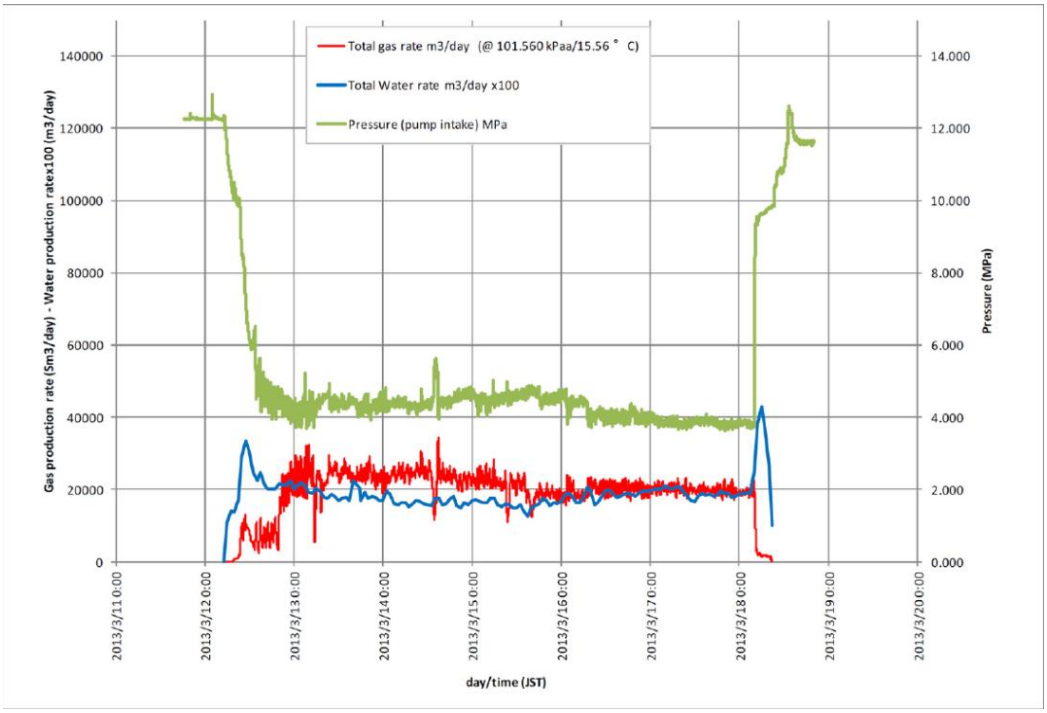

Fig 2.1.2 – Pressure data and gas and water production rates from the offshore field trial in the Nankai Trough (Yamamoto, et al., 2014).

2.1.3 Mallik

The Mackenzie delta/beaufort sea in Canada revealed sand layers saturated with 50-90% hydrate saturation during conventional hydrocarbon exploration. The gas hydrate was assumed to strongly contribute to the geomechanical stability of the formation. A production test was conducted in 2007 without implementing any form of sand control in order to investigate potential sediment inflow into the production well due to loss of formation integrity during hydrate dissociation. Significant inflow of sand was detected, thus the test ended after 24 hours. Another production test was conducted after implementing sand screens to reduce the sediment inflow into the production well. The test lasted for 6 days and gas production ranging from 2000 to 4000 m^3/day was maintained through the test (Grace, et al., 2008).

2.2 CO_2/CH_4 exchange in porous media

On a molecular level, the exchange process believed to occur through a solid-liquid-solid transformation. The methane hydrate melts momentarily at the hydrate/CO_2 interface, followed by the inclusion of CO_2 in the new hydrate. This happens inside the methane hydrate stability zone. Because $\Delta G<0$ in the exchange process, heat is released and push the methane hydrate nearby towards the phase boundary (Jung, et al., 2010).

Experiments done by Ersland et al. (2006) used MRI to monitor this exchange process. They used sandstone core sample which they cut in half lengthwise, and a 4mm polyethylene spacer was put in between the two half-cores. This spacer increased the surface area between the porous media and the hydrate former (methane), and could collect the produced methane from the exchange process. After the core was saturated with water and pressurized with methane, the system was cooled to 4°C to form hydrates. As the hydrates are formed, the MRI images show loss of signal and they clearly show were in the two core halves the formation takes place (Graue, et al., 2008).

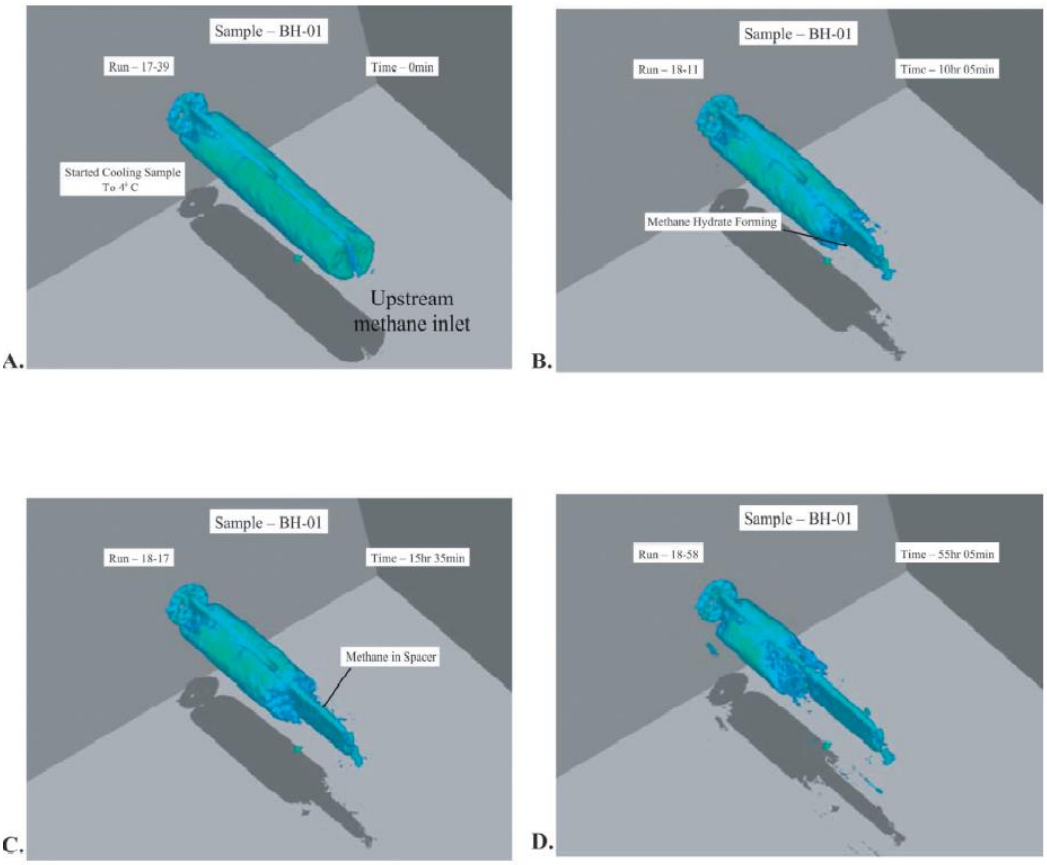

Fig 2.3.1 – Methane hydrate formation in the fractured core plug (Graue, et al., 2008).

After hydrate formation CO_2 was injected into the spacer. The MRI intensity across the spacer gave information about the amount of methane produced from the exchange process. After 4 days the methane concentration in the spacers stopped growing. 2-4 CO_2 flushes of the spacer was performed to increase the methane production. After 3 CO_2 flushes the total methane recovery was 50-85% of the gas originally in the hydrate plus all the free methane gas trapped in the pore space (Graue, et al., 2008).

2.4 Depressurization

A depressurization experiment reported by Ersland (2009) was conducted with a Bentheimer sandstone core with high hydrate saturation (61.7%) and formation water with low salinity (0.1%) (Birkedal, 2009). The production scheme used in the experiment was a constant pressure scheme and is similar to the depressurization procedure explained later in this thesis. After reducing the pressure close to the assumed dissociation pressure (42.9 bars) the pressure was reduced in 0.7bar steps. At 39.6 bar 9% of the methane was recovered. It was believed that low permeability limited the hydrate dissociation. Hydrate dissociation is an endothermic process which will absorb heat and may hinder further dissociation. The next pressure step (38.9 bars) gave a methane recovery of 47% after 96 hours. The last pressure step (38.1) produced rest of the methane resulting in a full recovery after a total experiment time of 280 hours.

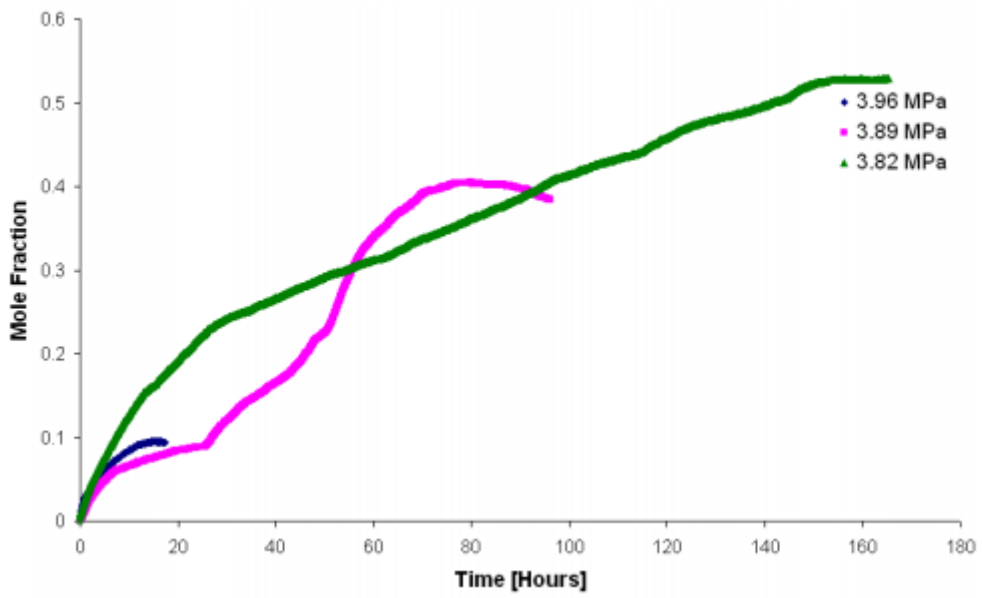

Fig 2.4.1 – Methane production from three pressure steps during depressurization (Ersland, et al., 2009).

Chapter 3 - Material and methods

Most of the experimental work was done at the hydrate core lab at the physics department at the University of Bergen (UiB). The experiments done at the hydrate core lab was done together with Stian Almenningen. One experiment was conducted with on the micro-lab together with Josef Flatlandsmo and one experiment was conducted at Statoil Sandsli together with Geir Ersland, Stian Almenningen, Josef Flatlandsmo and Håkon Juliussen. This chapter provides information about the porous media, the experimental setups and the experimental procedures.

3.1 Core Scale experiments

Experiments were conducted on 15 different cores at the hydrate core lab. Methane hydrate formation was performed in all of the experiments followed by gas production from most of the cores. CO_2 exchange was only performed in one of the experiments due to problems with the gas chromatograph. The purpose with these experiments was to gather more experimental data on hydrate formation and dissociation processes. A solid database is important to understand the nature of NGH. It is a helpful tool to find clear trends and to identify important and controlling parameters in the hydrate system.

Table 3.1 Overview of the core scale experiments, all done together with Stian Almenningen. The temperatures shown in the table is the temperature at the end of hydrate formation. For_2.1 and For_2.2 is two different experiments performed on the same core.

Core_id	PV [ml]	Swi [frac.]	Salinity [wt%]	Temperature[°C]	Production technique
CO2_33	69,67	0,685	3,5	4,0	CO2 exchange
Dep_6	71,01	0,670	3,5	1,5	Depressurization
Dep_7	70,81	0,585	3,5	2,5	Depressurization
Dep_8	68,29	0,697	3,5	2,5	Depressurization
Dep_9	70,49	0,663	3,5	0,0	Depressurization
Dep_10	72,39	0,677	3,5	4,0	Depressurization
Dep_11	69,95	0,691	3,5	0,7	Depressurization
Dep_12	70,90	0,668	3,5	4,0	Depressurization
Dep_13	70,99	0,662	3,5	4,0	Depressurization
For_1	71,55	0,648	3,5	0,2	Formation only
For_2.1	65,55	0,637	3,5	2,0	Formation only
For_2.2	65,55	0,637	3,5	4,0	Formation only
HR_57	69,15	0,664	3,5	4,0	Depressurization
HR_58	70,07	0,663	3,5	4,0	Depressurization

3.1.2 Experimental Setup

Three setups were used on the hydrate core lab, A, B and C. These setups have been used for several years by the hydrate research group at UiB. A list of equipment used and a schematic of the setup (*Fig 3.1.2c)* is found at the end of this section. Each setup consists of a cooling jacket with an integrated Hassler core holder. The temperature in the core holder is regulated with cooling bath that runs a coolant through the cooling jacket. The temperature is measured with an Omega Multilogger thermometer that is in contact with the core surface from the inlet, the outlet or both sides, depending on the setup.

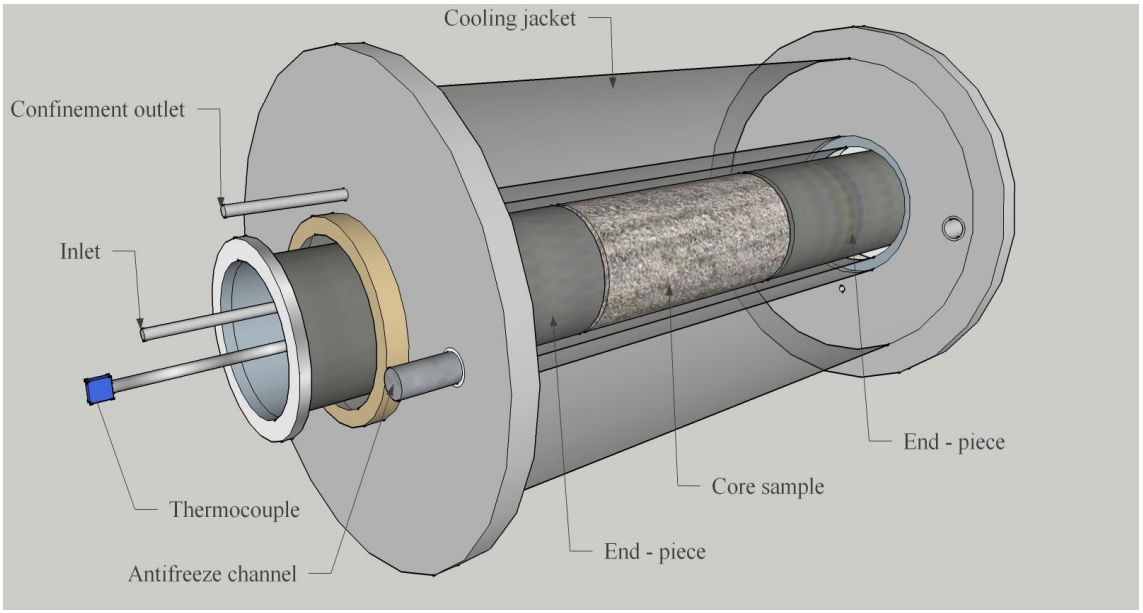

Fig 3.1.2a – Hassler core holder and cooling jacket. A rubber sleeve is wrapped around the core sample and end piece to separate the confinement oil from the porous media. The thermometer runs through the end piece and is in contact with the core sample (Hossainpour, 2013).

The end piece shown in *Fig 3.1.2b* is used in setup B and C, while setup A has floating end pieces. The floating end piece is pushed towards the core by the confinement oil. The end piece in Fig3.1.2b is screwed in contact with the core manually and does not depend on the confinement oil. Both kinds of end pieces have end piece channels that allow injection/extraction of fluids. The temperature sensor is also fitted through one of these end piece channels to get as close to the core as possible. A rubber sleeve is surrounding the core in all setups. The rubber sleeve provides a tight seal around the core, ensuring that the injected fluids do not bypass the core, but moves through it. The rubber sleeve in setup A is loose and is removed and cleaned between the experiments.

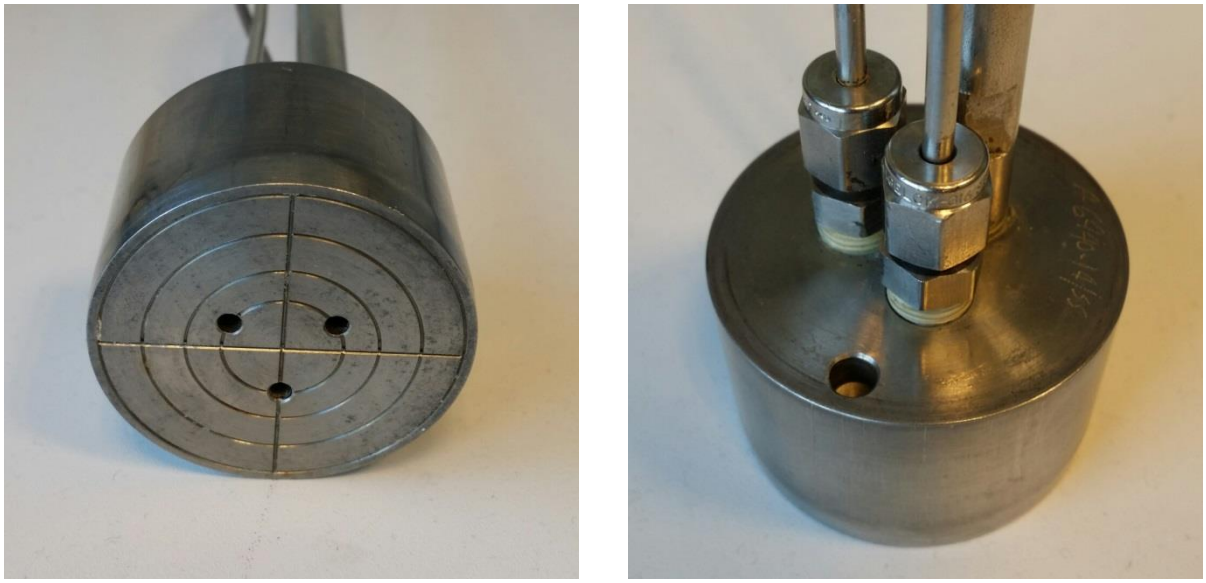

Fig 3.1.2b – (Left) shows the side of the end piece that is in contact with core on the inlet side in setup C. The three circular openings are channels that connect the core with the pump or a thermometer. (Right) shows the other side of the end piece on the inlet side in setup C. There are two 1/8 inch swagelock tubes that is connected to the end piece channel. The last channel is not used.

On the outside of the rubber sleeve in the core holder there is oil that can be pressurized to provide confinement pressure. An Isco pump is used to establish the desired confinement pressure, while a nitrogen buffer maintains the confinement pressure during the experiment. To pressurize the core itself, a high pressure pump (injection pump) is used. The pump is connected to the inlet and outlet end pieces through 1/8 inch tubing, after the core has been placed in the core holder. A bypass vent between the inlet and the outlet makes it possible to choose whether both sides is connected to the pump, or just the inlet. This makes it possible to pressurize/depressurize the core both sides or just one the inlet side. There is also pressure transducers mounted on inlet and outlet of the core holder, which main purpose is to measure the differential pressure across the core.

Between the bypass valve and the outlet valve, there is a valve connecting the outlet to a production line. The production line consists of various pressure regulators, water filters and investigative appliances in order to gather data from the fluid production in an efficient manner. To maintain the pressure in the core during production, a back pressure regulator (BPR) was installed after the production valve. The BPR is pressurized by a buffer to 85bar. After the BPR, there is a regulator that reduces the pressure of the produced fluids down to 1.5bar. A safety vent after the regulator ensures low pressure in produced gas before it reaches a gas chromatograph (GC). The pressure cannot exceed 2 bars in the GC without it breaking. A filter between the safety vent and the GC traps possible water and or unwanted particles in the production gas. The GC takes removes small gas samples from the production flow and analyses these to give the gas composition. At the end of the production line there is a mass flow meter that measures the weight of the gas passing through.

List of equipment used in the core scale experiments plus a schematic over the setups (*Fig 3.1.2c):*

- 3 x Hassler Core holder
- 3x Omega Multilogger HH506RA
- Grant LTC 6-30 cooling bath
- Thermo Neslab RTE-17
- 3x High pressure pumps (2x 1000ml, 1x 500ml), Sanchez Technologies
- Isco Series D pump
- 3x Cooling jackets made by the workshop at the physics department
- Back Pressure Regulator (BPR)
- Agilent Technologies 3000 Micro Gas Chromatography (GC)
- Bronkhorst Mini Cori Flow, Digital Mass Flow Meter (MFM)
- Water Trap
- Swagelok Pressure Regulator
- 2x Nitrogen Buffers
- 6x Unik Pressure Transducers
- Genie model 170 water filter
- Resistivity apparatus, HP 4262A LCR Meter

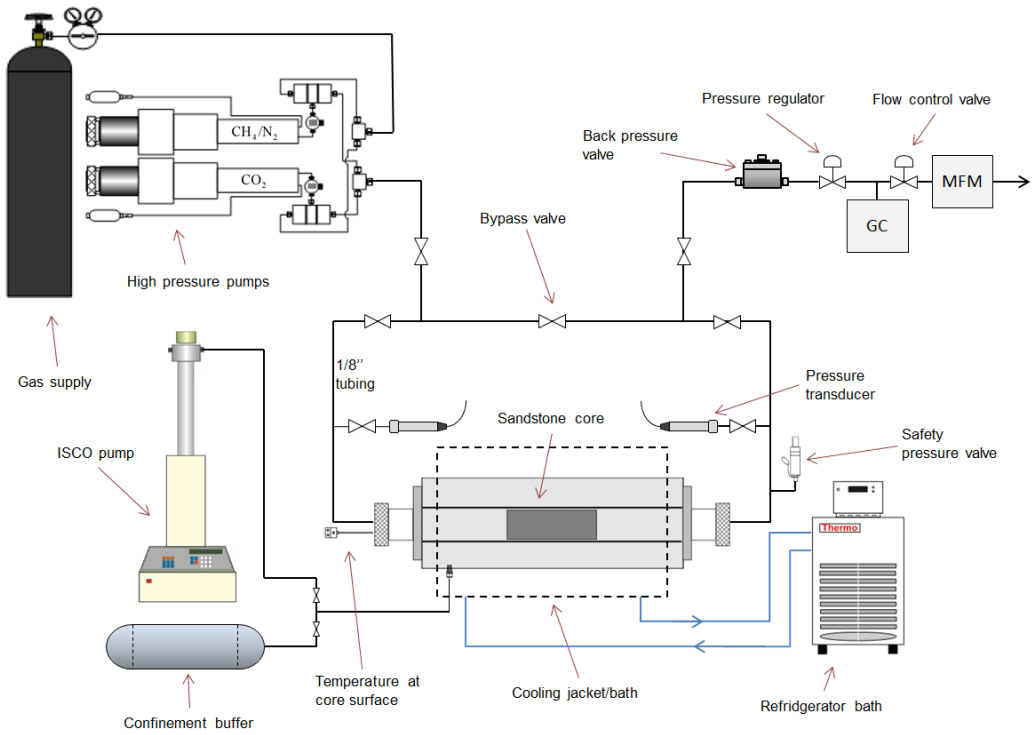

Fig 3.1.2c – Scheme of the experimental setups. Setup A, B and C share the production part, e.g the back pressure valve, GC and the MFM. Setup A and B is connected to the same confinement buffer and cooling bath. Setup A also has the possibility of resistivity measurements integrated. There are three high pressure pumps that deliver gas to the setups and regulate the pore pressure.

3.1.3 Modifications on the setup

After the first experiment, the GC stopped working. Some liquid water was probably carried out with the produced gas, and the GC broke down as a result. We installed a water catcher after the regulator. It can sustain pressures up to 8 bars, which is sufficient because the pressure between the regulator and the GC does not exceed 1.5 bars.

In setup C, an alternative flow path was installed due to problems with hydrate plugging. All of the core scale experiments had relatively high initial water saturation (55-70%) that resulted in free water after hydrate formation was finished. CO_2 comes in contact with the free water and can plug the system when initiating CO_2 sequestration. This path makes it possible to choose which end piece channel the gas will flow through. If plugging is indicated by a buildup in differential pressure across the core the gas flow will be redirected to the alternative path. If the pressure response returns after switching channels then there is likely a hydrate plug in the inlet end piece channel. If the differential pressure continues to build after the switch, then the plug is in the outlet end piece channel, the porous media or in the alternative inlet channel as well.

3.1.4 The porous media and core preparation

Bentheimer sandstone was used in all experiments. These outcrop core samples are gathered from a quarry in lower Saxony in Germany. It is a homogeneous rock with porosity ~ 23% and permeability ~1,1Darcy. It consists of 95-99% quarts and contains small amounts of the clay mineral kaolinite. The grain density is 2.65 g/cm^3. The outcrop has an average pore diameter of 125 microns (Birkedal, 2013). This stone is used because it is a good analogue to a real reservoir, and the relative low price compared to cores from real reservoirs.

Fig 3.1.4 – Bentheimer sandstone, cut to approximately 15cm in length and 5cm in diameter (Hågenvik, 2013).

The cores are approximately 15cm in length and have a diameter close to 5cm, if the diameter is larger than 5.20cm it will not fit in the core holder. After the core was cut into the appropriate size, they were put into an oven that held 60°C for 24 hours, this was to evaporate water remains in the core. The core was then weighed and the average length and diameter was obtained by measuring the length and diameter at three different places. Then the core was saturated with brine that had a salinity of 3.5 wt% NaCl. All experiments done in this thesis was done with relatively high water saturations (55-70%). This saturation was achieved by putting the core sample in a container, and

water was poured stepwise into the container to minimize the air trapped in the core. When the core was fully submerged it was kept there for 24 hours. Cores that were used in experiments involving CO_2 injection were wrapped in tinfoil before they were put into the core holder to protect the rubber sleeve from the acidic water and CO_2 mix.

3.1.5 Procedure for CH_4-hydrate Formation

After preparing the core as described in section *3.1.4*, the core was placed in the core holder. The confinement pressure was set to 30 bars. At this point the inlet and outlet valves were closed. The tubing and the pump was then vacuumed to get rid of as much air as possible. The system was now ready for methane pressurization. When the methane pressure reached 1bar the inlet and the outlet valves was opened simultaneously, and the core was now exposed to the methane. The system was pressurized to 83 bar, and the confinement pressure was always kept at least 30 bars above the pore pressure. With the injection pump at constant pressure at 83 bars, the system was monitored for 24 hours to check for possible leakage. The system was now cooled to 4°C. The injection pump was still kept on constant pressure, and the system was kept like this for 10-16 days until the rate of methane injection approached 0. After the hydrate formation the volume and pressure data from the pump log was used to calculate important parameters:

Volume of hydrate formed:

$$V_H = \frac{V_{CH4}^H * \rho_{CH4} * M_w^{water} * 7{,}547}{M_w^{CH4} * \rho_w} \qquad (3.1.5a)$$

In *eq. 3.1.5a* V_H is the hydrate volume and V_{CH4}^H is the volume of methane consumed during hydrate formation. ρ_{CH4} and ρ_w are the densities of methane and water respectively, at 83 bar and 21°C. M_w^{water} and M_w^{CH4} is the molar weight of water and methane, respectively. 7,547 is the product of the hydration number (5.99) and the water expansion factor (1.26). Because water expands when forming hydrates, some of the gas will be pushed away. This results in an underestimation of V_{CH4}^H, which leads to an underestimation of the hydrate saturation. To address this problem, iteration was executed, where the number of moles of methane pushed away by the expanding water was added to the number of moles of methane that takes part in the hydrate formation.

Weight % NaCl in the free water after hydrate formation:

$$w_{NaCl}^{\%} = \frac{m_{NaCl}}{m_w^i - \left(n_{H2O}^h * M_w^{water}\right)} \qquad (3.1.5b)$$

When hydrates are formed the salt in the water is not included in hydrate structure. This leads to an increase in the salinity as the hydrates grow. m_{NaCl} is the mass of NaCl and is constant throughout formation. m_w^i is the mass of initial brine. n_{H2O}^h is the number of moles included in the hydrate formation. M_w is the molar mass of water.

3.1.6 Procedure for CO_2/CH_4 – Exchange

Due to trouble with the gas chromatograph only one exchange experiment were conducted, CO2_33. After following the procedures described in section *3.4* and *3.5* two injection pumps was prepared to co-inject a mixture of CO_2 (40%) and N_2 (60%) with a flowrate of 4ml/hour. Pure N_2 was injected for 4 hours with a flowrate of 5ml/ before initiating the injection of the mixture. The purpose of the pure N_2 injection was to flush out the methane gas in the tubing, and to prevent hydrate plugging by displacing possible free water residing in the near end-piece area. Co-injection of the gas mix (40/60) was initiated with the flush-sequence described in *Table 3.1.6.* The flush-sequence was chosen instead of a constant injection scheme because the former makes it easier to process the output data from the GC. A flush-sequence also makes it more convenient to monitor the differential pressure across the core because of the relatively short injection intervals. After each flush the pump was stopped and the inlet and outlet valves to the core were closed. When initiating the next flush after a pause, the pressure in the pump was set to match the core pressure before opening up the inlet and outlet valves.

Table 3.1.6 – Overview of the flush-sequence used in CO2_33. The injected gas mix was kept constant at CO_2 (40%) and N_2 (60%)

Flush #	Injection rate [ml/hour]	Injection time [hours]	Pause [hours]
1	2	3,2	23,3
2	2	4,3	22,0
3	4	5,0	13,0
4	4	5,8	18,5
5	6	8,0	16,0
6	6	8,8	16,5
7	6	2,5	24,5
8	6	5,0	18,7
9	6	5,0	--

Information about the gas production from each of the CO_2/N_2 flushes was found through the GC and MFM. The composition and the mass of the gas produced were used to calculate the moles of methane produced and the recovery factor.

3.1.7 Procedure for Depressurization

After carrying out procedure *3.4* and *3.5* the pressure in the core is lowered to 48 bars. This step is done with a relatively low drawback rate from the pump, between 1.5 – 0.5 ml/min, this is to avoid production of the free water in the core. The pressure reduction is done with the bypass valve open so that the pressure will decrease equally from both inlet and outlet. This is to prevent a huge differential pressure across the core. The bypass valve is now shut and small pressure steps, 0.7 bars each, is conducted. The pump is set to constant pressure for about 24 hours after each pressure step, or until the flowrate of the pump is close to zero. When the core pressure reaches 30 bars, a large pressure step down to 22 bars is conducted to make sure all the hydrates have dissociated.

3.1.8 Flow Testing

Because of some problems with hydrate plugging in the early experiments, a permeability test was conducted on dep_13, HR_57 and HR_58. Instead of following the regular depressurization procedure with lowering the pressure from 83 to 48 in one big step with the bypass vale open, the bypass valve was kept closed and the pump was set to draw back 0.1 ml/min. This was done to see if there was any pressure response between the inlet and outlet transducer. The pressure in dep_13 was reduced to 66 bars with the bypass valve closed. HR_57 was first reduced to 70 bars and set to constant pressure over night and was further reduced to 60 bar the next day. When the pressure reached 60 bars the pump was again set to constant pressure.

3.1.9 Resistivity measurements

Resistivity measurements were used as a logging tool due to the difference in electrical conductivity between brine and hydrates. Theory states that the resistivity will increase as the hydrates saturation increase above 20%. The resistivity data would then be a helpful tool to distinguish between processes such as hydrate formation and leakage. The resistivity measurements were conducted on setup A. the reason was because the floating end piece is only in contact with the (isolating) rubber sleeve and the core sample, while the other kind of end piece is also in contact with the (conducting) core holder. A LCR meter was connected to the inlet and outlet of the core vessel. The resistance of the current loop was read by a web camera taking picture of the LCR display. The resistance value was then transferred from the pictures to a computer. This process was time consuming, but the best option due to interference in the current when connecting the LCR meter to a computer. The resistivity was then obtained by *Equation 3.4.3***.**

$$R_t = r \cdot \frac{A}{l} \tag{3.4.3}$$

R_t is the total resistivity across the core, r is the measured resistance, A is the cross sectional area of the core and l is the core length.

3.2 MRI of hydrate, experimental setup and procedure

Together with the hydrate research group MRI experiments was conducted on a Bentheimer sandstone core at Statoil Sandsli's new hydrate lab (2015). The purpose of the experiments was to get acquainted with the MRI apparatus by conducting a series of basic experiments. Two different processes were imaged; one-phase flow and hydrate dissociation. The setup consisted of an MRI apparatus and an independent cooling unit. The laboratory used in these experiments is still developing. Pressure cells have not been installed yet and the experiments where therefore conducted under atmospheric pressure thus cyclopentane was used as hydrate former. During the one-phase flow experiment plastic tubing were connected to the inlet and outlet of the core, and flow was controlled by an injection pump. A Bentheimer sandstone core was cut to 15cm. The core was placed in an oven for 24 hours to dry. Two plastic end pieces were fitted to the core. Epoxy glue was applied to the core sided to make a seal (*Fig 3.2)*. The Epoxy glue was also used to fasten the end pieces.

Fig 3.2 – A Bentheimer sandstone core sealed fitted with plastic end pieces and covered in epoxy glue. The scale in the picture is in cm.

The core and brine (5wt% NaCl) was separately in two air tight cells connected to a vacuum pump. After being evacuated for approximately 2 hours a vent between the two cells were opened. The brine flowed into the cell were the core resided to imbibe the porous media to until 100% S_w was obtained. The core was connected to an injection pump filled with cyclopentane after the one-phase flow experiments were conducted. Cyclopentane was injected until no water was observed in the fluid production. The target saturation was residual cyclopentane saturation thus brine was injected until no more cyclopentane was observed in the fluid production.

The first experiment was initiated by placing the 100% water saturated core into the magnetic field in the MRI apparatus and flow was initiated by an injection pump filled with deuterium-oxide (heavy water). The hydrate dissociation experiment started with the same core with residual cyclopentane saturation. The core was put in a refrigerator and cooled to 2°C which is within the stable zone for cyclopentane hydrate. The core was wrapped in bubble wrap to delay the dissociation process. The core was then placed inside the MRI apparatus and an image interval of 1 hour was initiated.

3.3 Pore Scale Hydrate Growth

Two micro model experiments were conducted together with Josef Flatlandsmo. The goal for these experiments was to look at hydrate growth at pore scale, to see where in the porous media hydrates grow and to see how the system of water, methane and hydrates behave during growth. Minor modifications have been done on the setup used and build by Høyland (2014).

3.3.1 Pore Scale Equipment and setup

The micro model setup consisted of a thin slice of silicon wafer replica of a porous media (micro model) submerged in cold water. A camera was placed on top of a microscope with view of the micro model. A high precision pump, consisting of two cylinders filled with water and methane, was connected to two of the micro model corner channels. A pressure transducer was connected to one of the available corner channels during pressure testing of the model. An outer chamber around the

micro model contained coolant connected to a cooling bath. The following is a list of equipment used and a schematic of the setup (*Fig 3.3.1).*

- High pressure micro model based on Berea sandstone
- A micro model cover
- A container with two separate chambers, from the UiB workshop
- Thermo Neslab RTE-17refrigerated circulating bath
- Quizix SP-5200 pump system
- Nikon SMZ 1500 microscope
- Nikon D7100 camera
- Photonic optics LED-F1 cold light source
- Pressure transducer

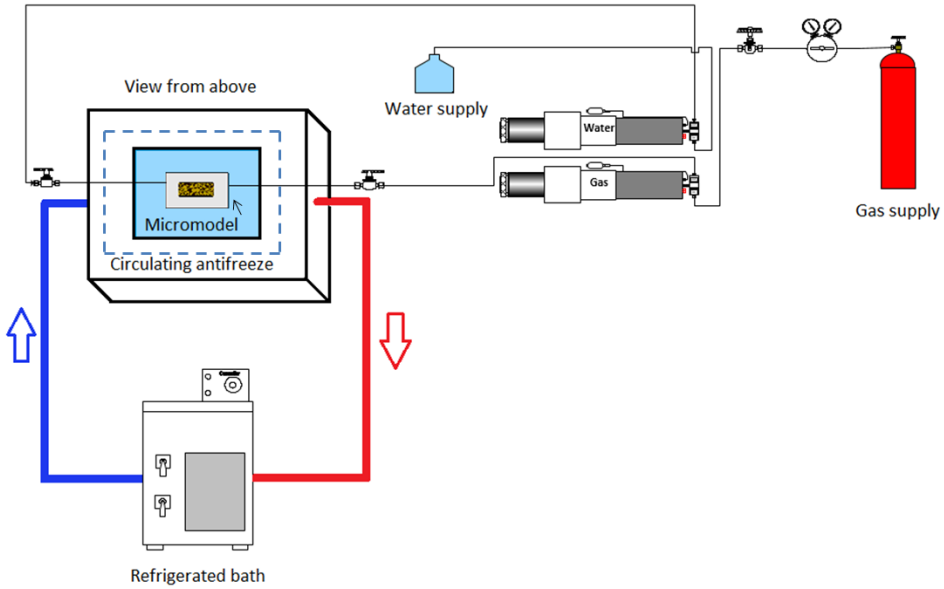

Fig 3.3.1 – Experimental setup illustrated from above. The pump system consists of two cylinders which are filled with distilled water and methane gas. The coolant flows through the outer chamber and in that ways cools the water in the inner chamber. Figure from (Høyland, 2014).

The modifications done on the setup includes a new and more reliable cooling bath and an extra computer screen making it possible to look at live images from the micro model and live pump data simultaneously. A pressure transducer was connected to the micro model while pressure testing the system prior to the experiment. A more detailed description of the setup and its components can be found in (Høyland, 2014)

3.3.2 The Micro Model

The micro model is a thin silicon wafer replica of porous media. The ones used in this experiment are manufactured by PharmaFluidics. The model is constructed in five steps: (1) a high resolution photograph is taken of a thin section of a porous media, in this case Berea sandstone. (2) The photograph is now digitally manipulated so that the resolution of the image is good enough to get all

the details of the flow path. (3) An image mask is now constructed; this mask yields an exact 2D replica of the original pore network. (4) A silicon wafer is coated with a photoresist material and placed onto the image mask so that the coated side is in contact with the mask. UV-light is shined through the mask and burns the pore structure into the silicon wafer. (5) To reach proper wettability the silicon wafer is oxidized. A glass plate with inlet and outlet ports is fitted, and the bottom is coated with epoxy for increased strength (Hornbrook, et al., 1991).

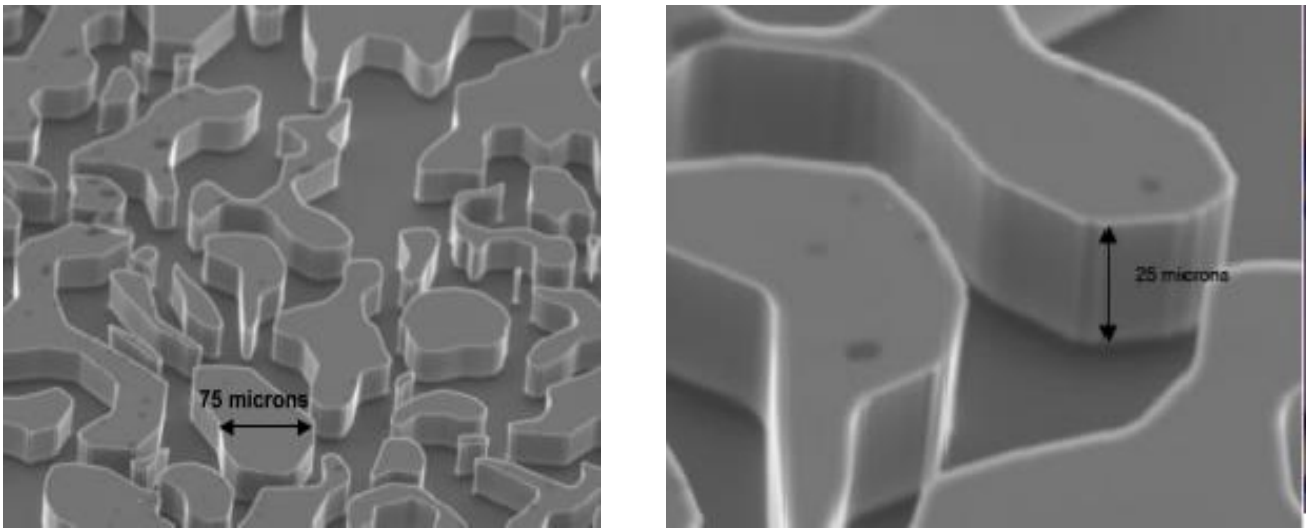

Fig 3.2.2a – To the left we see a scanning electron microscopy image of the pore network in the micro model. The right image is taken at a 45° angel and shows the depth of the model (Rangel-German & Kovscek, 2006)

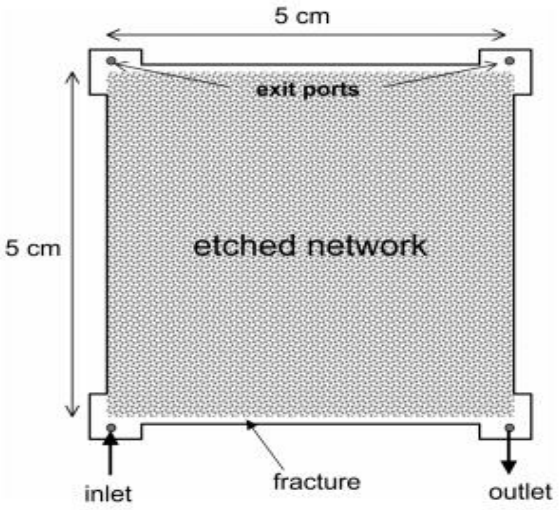

Fig 3.2.2b –.A schematic of the micro model (Rangel-German & Kovscek, 2006).

3.3.3 Procedure for Pore Scale Hydrate Growth

Distilled water and methane gas was mix together in the two pump cylinders. The initial temperature in the micro model was 13°C thus outside the hydrate stabile zone. The system was pressurized to 83 Bars. At this point no gas bubbles were present in the micro model, at least not in the field of view of the camera. Flow was initiated through the model to get gas bubbles within the field of view. When both water and free gas were present in the model and could be observed through the camera and microscope the system was ready for cooling. The cooling bath was set to 2 degrees, and the camera was set to take 1 picture each minute. The camera was set to record video as the conditions in the micro model approached the expected interval of hydrate formation.

Chapter 4 - Results and Discussion

This chapter provides the results from the experimental work together with a discussion of these results. Further sections in the chapter include hydrate formation, hydrate growth, final hydrate saturation and a discussion of uncertainties. The results in this thesis will be compared to earlier work done on NGH at the Department of Physics and Technology. The results from the pore scale experiment will not be presented in a separate section, but is used to support the results in the hydrate growth section. Experiment conducted in this thesis will be referred to as new experiments.

4.1 Hydrate Formation

Hydrate formation experiments was carried out in all experiments prior to the production schemes. Investigation of hydrate formation in the lab may lead to higher precision in predicting energy potential in hydrate deposits, due to an increased knowledge of growth patterns and hydrate saturations. The data from the experiments was obtained from the injection pump log (pressure, volume and injection rate), resistivity measurements, temperature log and from pressure transducers. These data were processed to obtain results including induction time, growth rate and final fluid saturations. *Table 4.1* below will provide an overview of the experiments conducted along with key results from hydrate formation.

Table 4.1 – A list of the experiments conducted on the hydrate core lab along with key results from the hydrate formation. *Induction time.

Core_id	Swi [frac.]	Temp. [°C]	Salinity [wt%]	S_{hydrat} [frac.]	S_{wf} [frac.]	S_{gas} [frac.]	Setup	t_i* [hours]
CO2_33	0,69	4,0	3,50	0,59	0,31	0,21	B	5,40
Dep_6	0,67	1,5	3,50	0,45	0,32	0,23	C	2,75
Dep_7	0,59	2,5	3,50	0,51	0,17	0,30	A	1,70
Dep_8	0,70	2,5	3,50	0,48	0,32	0,19	B	1,90
Dep_9	0,66	0,0	3,50	0,64	0,14	0,19	C	6,20
Dep_10	0,68	4,0	3,50	0,52	0,28	0,21	A	3,38
Dep_11	0,69	0,7	3,50	0,61	0,21	0,17	B	2,00
Dep_12	0,67	4,0	3,50	0,56	0,23	0,21	B	35,50
Dep_13	0,66	4,0	3,50	0,54	0,24	0,22	C	15,20
HR_57	0,66	4,0	3,50	0,54	0,25	0,22	A	2,40
HR_58	0,66	4,0	3,50	0,53	0,25	0,22	A	4,30
For_1	0,65	0,2	3,50	0,49	0,22	0,23	C	2,94
For_2.2	0,64	4,0	3,50	0,53	0,23	0,25	B	1,75
For_3	0,57	2,0	3,50	0,40	0,25	0,34	B	1,00
For_4	0,57	2,0	3,50	0,50	0,19	0,32	A	2,00

The hydrate formation curve of CO2_33 is shown in *Fig 4.1a*. The methane consumed by hydrate formation is plotted against time together with the core temperature. The graph shows the cooling and the induction period (5.4 hours) followed by an initial rate of hydrate formation. The hydrate formation rate is gradually decreasing until it reaches the final rate of formation. A total methane consumption of 59ml was reached after approximately 400 hours. An important comment is that the

methane consumed in this plot, is actually the methane injected. The methane injected is the methane consumption due to hydrate formation + the methane injected due to gas contraction during the cooling period. In CO2_33 the value of injected gas due to cooling is 2.5ml. The red line in *Fig 4.1a* shows the temperature. CO2_33 was the first experiment conducted in the thesis which led to a stepwise lowering of the temperature due to uncertainties regarding the isolation of the flow loop. The core temperature stabilized around 4°C after approximately 38 hours.

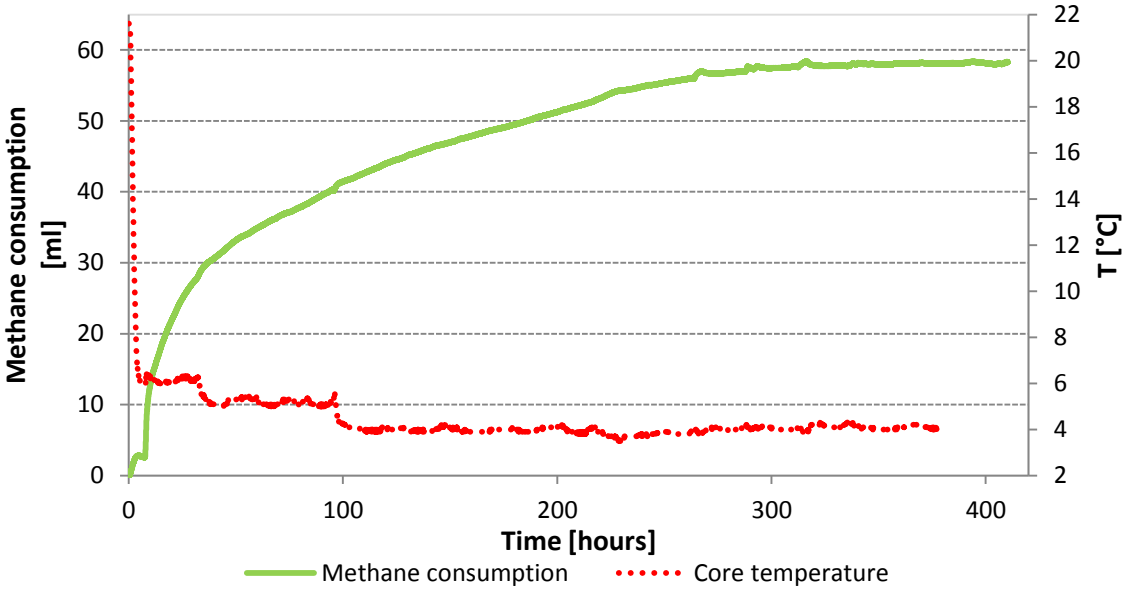

Fig 4.1a – Hydrate formation of the CO2_33 experiment. The green line represents the methane consumption, and the red line is core temperature, measured at the inlet side of the core. The leakage rate is 0.015ml/hour and the leaked volume is subtracted from the consumed gas.

The hydrate formation curves from the experiments listed in *Table 4.1 are* shown in *Fig 4.1b*. This figure illustrates the range of methane consumption and the different shapes of the formation curves. Hydrate formation in 15 different core samples were successful and provide statistical data to the in-house database. The initial salinities in the formation water in all of the experiments were 3.50 wt%. The initial water saturation varied relatively much even though the saturation procedure was also kept constant between the experiments and Bentheimer Sandstone cores was used in all of them. S_{wi} ranged from 0.57 – 0.70, thus indicating a difference in pore size distribution, the width of the pore necks or matrix composition, between the cores. The average pore size is ~125 µm. A relative high fraction of small pores (< 125 µm) leads to higher S_{wi} due to a higher pore wall/pore space ratio which causes a stronger capillary drive, assuming water wet porous media. Another important parameter is the temperature. The temperatures given in *Table 4.1* are the temperatures at the end of hydrate formation. There was a variation from 0 - 4°C between the coldest and warmest experiment. Lower temperature gives higher driving force towards hydrate formation. The significance parameters mentioned above will be discussed more thoroughly in the sections ahead.

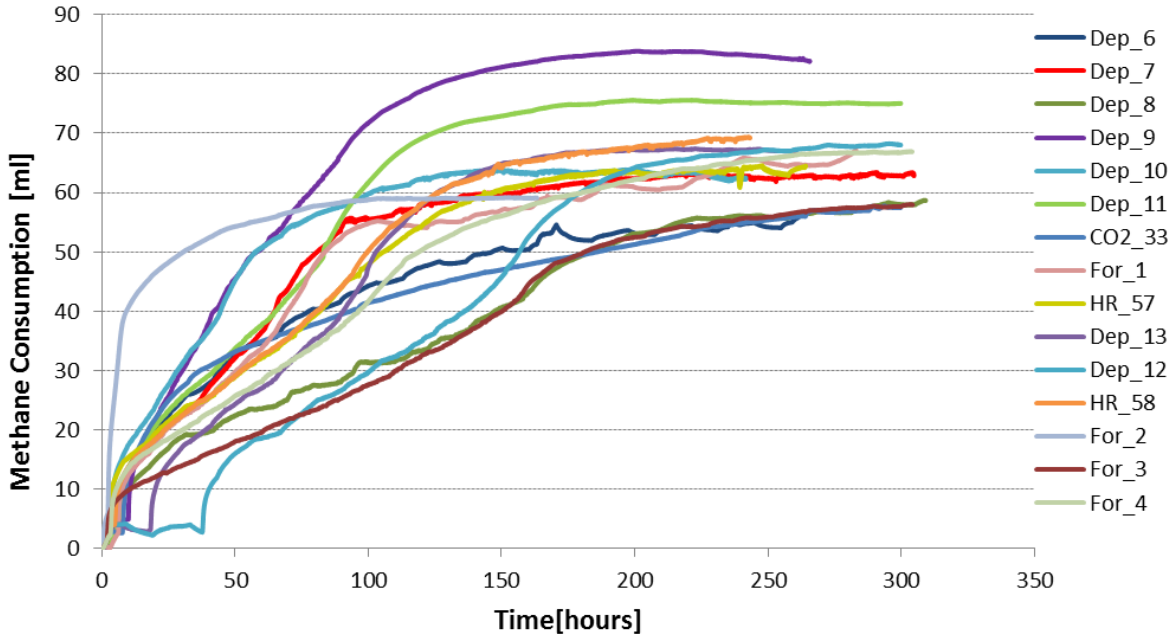

Fig 4.1a – Formation curves for all the experiments listed in *table 4.1*. The cooling – and the induction period is part of the methane consumption in the graph, but is excluded from the hydrate saturation calculations.

4.1.1 Induction Time

The induction time is the time period in which the conditions in the system are within hydrate stable zone, but hydrate growth is not detected. The induction times spread over a wide range (1 – 35.5 hours) amongst the experiments. This section discusses possible reasons for this large interval of values in induction time.

Fig 4.1.1a shows the first 15 hours after cooling of the CO2_33 core is initiated. The dashed red line in shows a temperature reduction from 22°C to 6°C. The green line, representing the volume of gas injected, is increasing as a result of the temperature change. The induction time is found by subtracting the time it took for the core to reach 12°C (1) from the time where the rate of gas injection suddenly increases (2), thus finding the amount of time the system is within the hydrate stable zone without any hydrates being detected. 12°C is used as hydrate stable boundary temperature for all the cores when calculating the induction time. *Fig 4.1.1a* shows that the core temperature was 6°C during the induction time. The target formation temperature was 4°C. The extra 2°C lowers the driving forces and has may have caused a prolonged induction time.

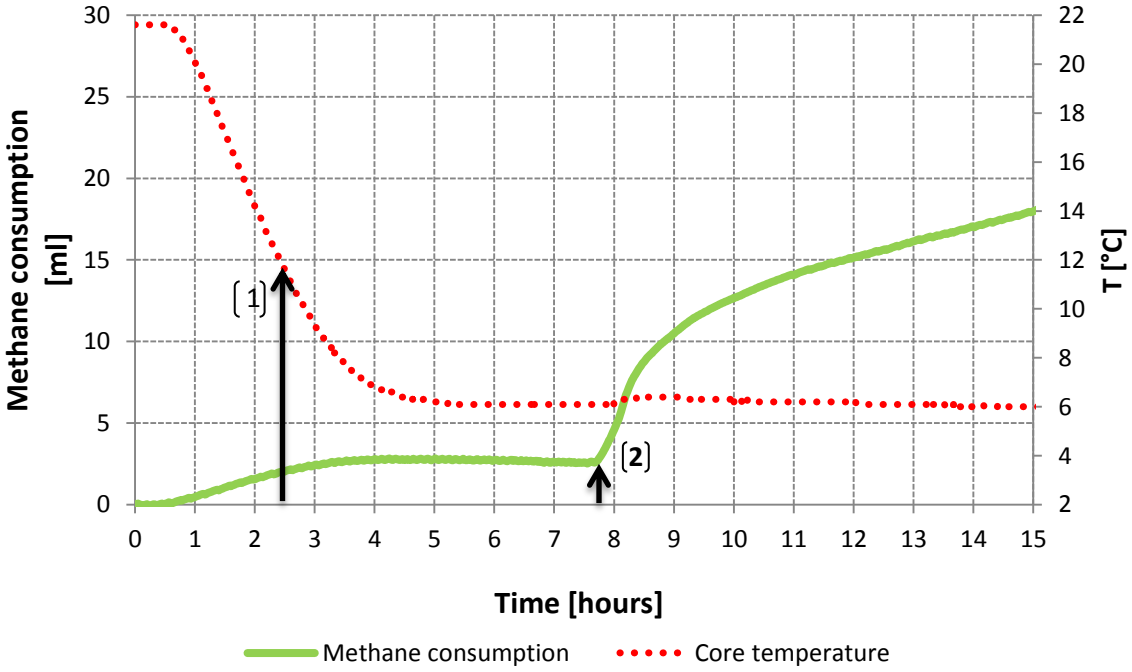

Fig 4.1.1a – First 15 hours after initiating cooling of CO2_33**.** (1) indicates the time the core temperature was at 12°C. (2) indicates initial hydrate formation, thus the end of the induction period. The methane injected due to cooling is excluded when calculating the hydrate saturation.

As *Fig 4.1.1b* shows the induction times plotted against core temperature for the experiments listed in *Table 4.1*. A relatively small range of induction times (1.00 - 6.20 hours) was observed for the experiments with temperature from 0-2.5°C. The experiments with 4°C core temperature had a much larger range (1.75 – 35.50 hours). Dep_12 and Dep_13 had a much longer induction time than the other experiments. Because of the stochastic nature of hydrate formation, a range of different induction times was expected, but a 35.50 hour induction time at the actual conditions is unusual. Dep_12 has approximately 10 times the induction time as the average. One experiment in the in-house database had a longer induction time than Dep_12. This was CO2_24, and was conducted by Truls Hamre Håheim and Reza Hossainpour (2013). In this experiment the core temperature was kept at 9.6°C during the first stage of the hydrate formation. After 70 hours within the stability region no hydrate formation was observed. After lowering the temperature further to 4°C, the hydrate formation started immediately (Hossainpour, 2013). There is no clear correlation between temperature and induction time within the 0-4°C, but the temperature may have a more significant impact closer to the hydrate stability line.

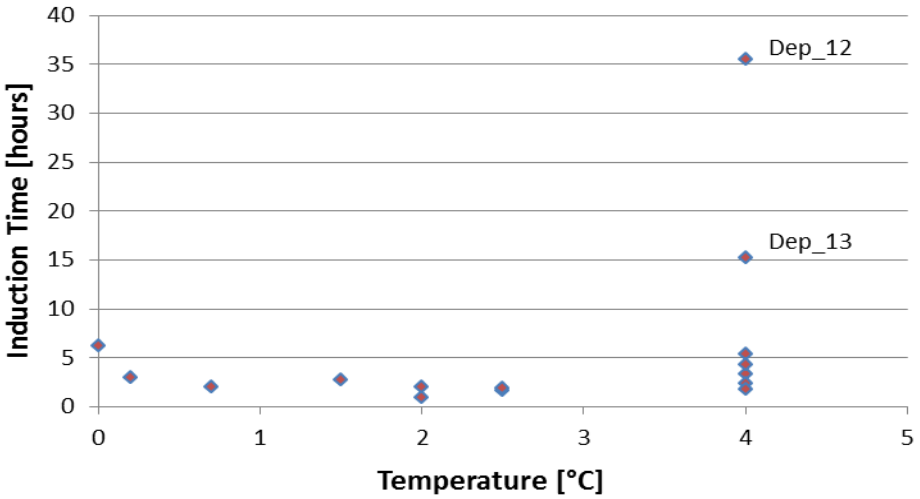

Fig 4.1.1b – Induction time plotted against temperature. The temperature in the plot is the temperature at the end of the formation.

Another parameter in hydrate formation is S_{wi}. Assuming that the saturation process and the matrix composition for all the cores was identical and that the pore necks was proportional to the pore size; the initial water saturation would mainly depend in the pore size distribution. A high amount of large pores would give a relatively small S_{wi}, due to a decreased capillary drive. Hydrates tend to form at the gas/liquid interface, were the mass and heat transport are sufficient. In water-wet sandstone like Bentheimer, the water is drawn to the pore wall therefore gas will often reside in the larger pores, thus hydrate formation will most likely take place in the larger pores (Kleinberg, et al., 2003). Assuming that larger pores leads to lower initial S_{wi}, one can argue that lower S_{wi} gives shorter induction times due to a larger interfacial area between methane gas and liquid water. *Fig 4.4.1c* shows a trend to support this argument. Dep_12 and dep_13 is not part of the plot due to their abnormally high induction times. The temperature also varies between the experiments in the plot, but the temperature showed little significance on induction time in the investigated range (0-4°C.)

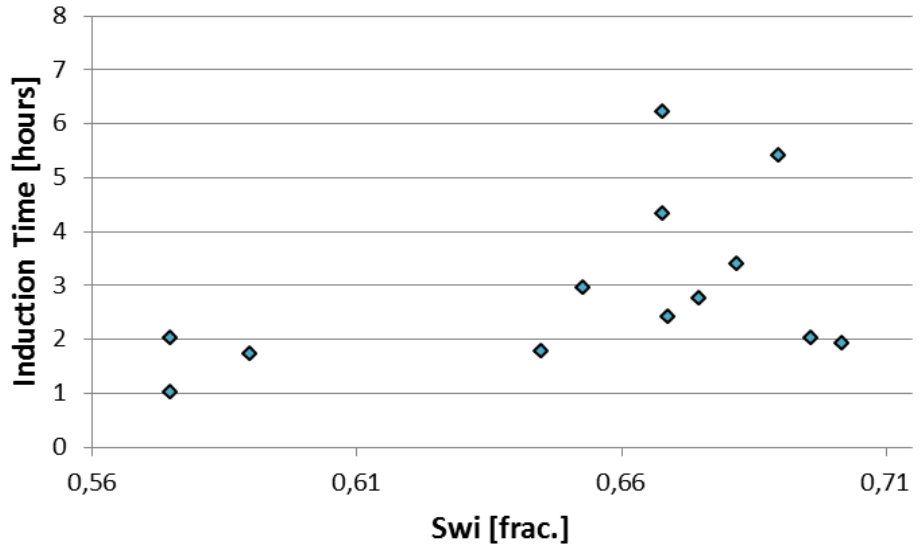

Fig 4.1.1c – Induction time plotted against initial water saturation for. Dep_12 and Dep_13 have been left out due to the abnormally long induction times.

The first 50 hours of the hydrate formation in Dep_12 was plotted to examine the induction period for any abnormalities (*Fig 4.1.1d).*The cooling period (1) progressed as expected, and there was correlation between the temperature drop and volume response. After approximately 10 hours the is a methane consumption rate becomes negative, and 2 ml of methane is retracted, before the rate turn positive (2). The injection pump is set to maintain a constant pressure during the hydrate formation, therefore it responds to pressure changes. No change in temperature was observed during the induction period. After supposedly being within the hydrate stable zone for 35.50 hours, the rate suddenly increased (3) which indicate hydrate formation.

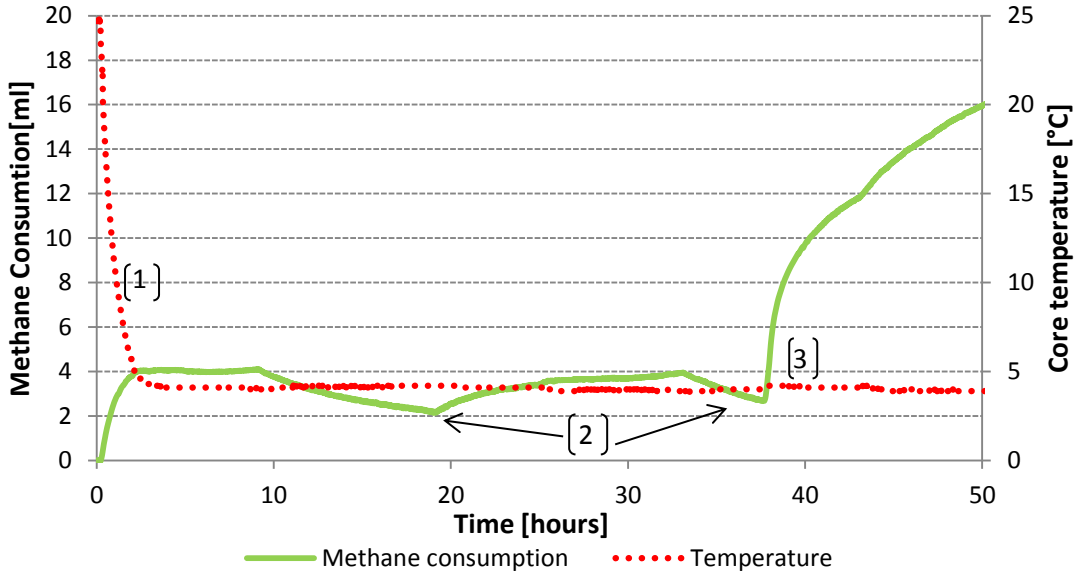

Fig 4.1.1d – First part of the hydrate formation in Dep_12. This experiment had the longest induction time with 35.5 hours. (1) Cooling, (2) two abnormalities in the methane consumption (3) sudden increase in methane consumption rate.

The induction period can also be recognized from the resistivity measurements. As cooling of the core begins; the resistivity of the core sample increases along with the methane injection. The resistivity and methane injection flattens out as the core reaches its set temperature. At this point there is no hydrate growth in the core even though the conditions are within the hydrate stable region. As Fig 4.1.1e shows there is a sudden drop in resistivity just before massive hydrate growth starts. Birkedal (2011] observed this resistivity drop in a series of experiments on hydrate formation. The resistivity drop was first believed to be caused by adiabatic heating during the initial hydrate growth. Birkedal registered minor temperature variations of 0.5°C. A slight temperature increase was observed in HR_58 (0.4°C) but no change was seen in HR_57. The initial cooling was from 24°C to 4°C and the corresponding resistivity increase was 5Ωm, therefore it is not likely that an increase of 0,5°C should cause a 2,5 Ωm drop in the resistivity. Birkedal concluded that the effect was most likely a combination of the temperature increase, elevation of the ion concentration at the gas/water/hydrate interface, variation in hydrate morphology and differences in hydrate growth patterns.

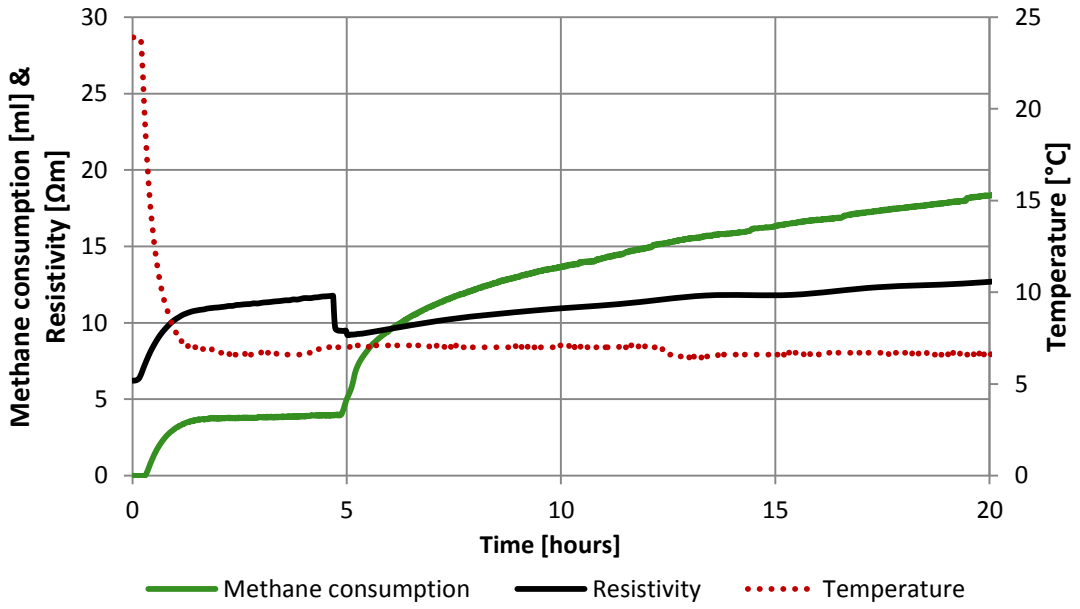

Fig 4.1.1e – First 20 hours of hydrate formation in HR_58. The initial temperature drop induces a response in the resistivity and the methane volume. An increase in methane consumption and a drop in resistivity just before the 5 hour mark display the end of the induction period. There is an offset of +2.5°C in the temperature output, the real temperature in the core is approximately 4°C.

4.1.2 Hydrate growth

The shape of the formation curve can provide information about growth kinetics which depends on the mass- and heat transport and the intrinsic kinetics. Due to the salinity of the initial formation water we expect a relatively long growth period compared to previously low salinity (0.1 wt%) experiments conducted . The salt lowers the activity of the water which results in a shift in the hydrate stability curve towards higher pressure and lower temperature. As hydrates form, the salinity in the formation water increases. Various salinities have been used in earlier experiments done by the hydrate research group and the difference in hydrate growth rate can be seen in *Fig 4.1.2a.*The hydrate growth rate in the cores with 0.1 wt% of NaCl is higher than the cores with 3.5 wt% NaCl. Another observation from *Fig 4.1.2a* is the abrupt transition from high rate of consumption to almost no methane consumption at all on the low salinity experiments. On the high salinity experiments there is a much smoother transition. An explanation for this behavior might be that as hydrates are formed in the high salinity cores, the salt concentration in the water left in the pores increases and therefore slows down further hydrate formation. In the low salinity cores on the other hand, this effect will be less significant because of the low initial salt concentration, and hydrates will keep forming at a high rate until it runs out of either gas or water. Because this is excess gas experiments there is always enough gas present, but as hydrates are formed, the permeability in the core is reduced and the gas might not reach every part of the core.

Table 4.1.2 – Core data from the previous experiments used in Fig 4.1.2a and b below.*Ersland, Birkedal & Hauge.

Core_id	PV [ml]	Swi [frac.]	Temp. [°C]	Salinity [wt%]	Personnel
CO2_05	67,30	0,52	4,0	0,1	Birkedal
CO2_08	75,46	0,56	4,0	3,5	Birkedal
CO2_09	68,59	0,51	4,0	3,5	Birkedal
CO2_11	70,62	0,41	4,0	3,5	Birkedal
CO2_15	72,81	0,41	4,0	0,1	Birkedal & Hauge
CO2_17	68,01	0,41	4,0	0,1	E, B & H*
CO2_18	66,63	0,41	4,0	0,1	E, B & H*
HR_10	64,12	0,65	4,0	3,5	Birkedal
HR_38	69,40	0,50	4,0	3,5	Hauge & Birkedal
HR_39	65,47	0,47	4,0	3,5	Hauge & Birkedal
HR_46	64,71	0,40	4,0	3,5	Hauge & Birkedal
HR_47	68,96	0,42	4,0	3,5	Berge & Hågenvik
HR_48	62,10	0,40	4,0	3,5	Berge & Hågenvik

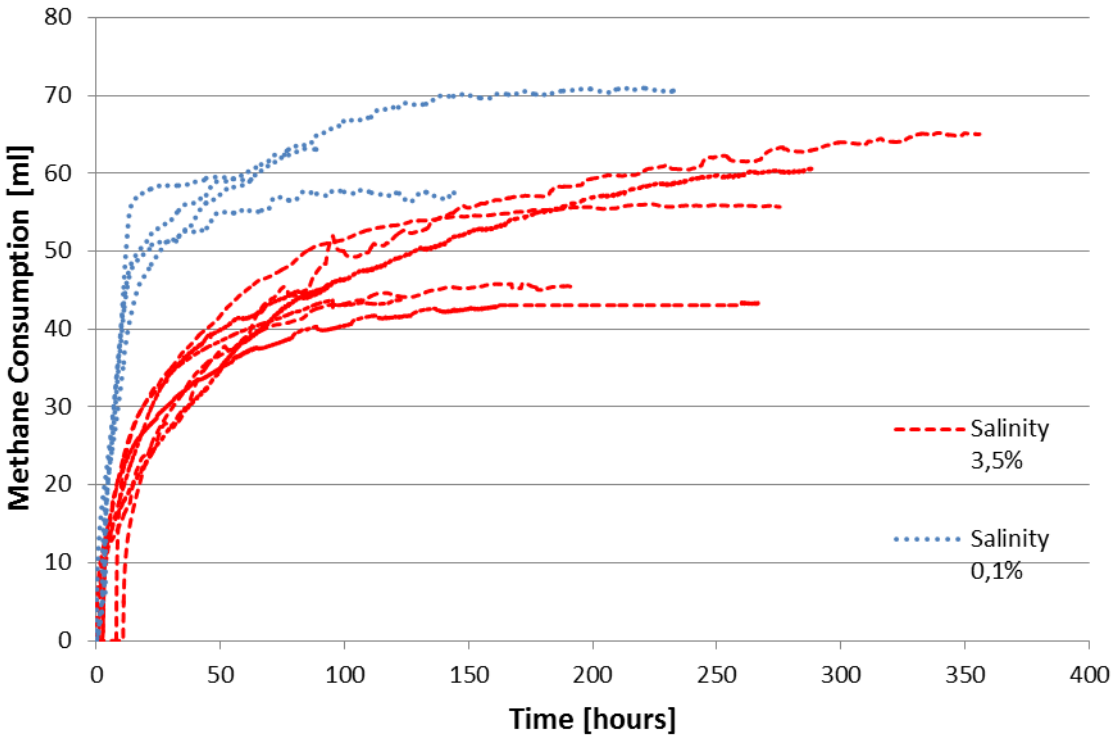

Fig 4.1.2a – Comparison plot between hydrate formations with different salt concentration. The red and blue lines represent formation curves done with 3.5 and 0.1 weight % respectively. These experiments were conducted by Birkedal, Hauge, Berge and Hågenvik in 2013.

When plotting previous experiments together with 4 of the new experiments, *Fig 4.1.2b* show that the new experiments (green solid line) is close to the high salinity experiments done earlier (red dashed line). The two green formation curves with highest methane consumption (Dep_7 and Dep_10) have a shape that resembles the low salinity experiments, which is a more abrupt transition to the final growth rate, compared the other experiments done at 3.5% salt concentration.

The S_{wi} values in the previous experiments are generally lower than in the new experiments (*table 4.1.2)*. As mentioned the previous section; High S_{wi} indicates larger amounts of small pores, thus a larger fraction of the pore space is occupied by water, and the water/gas surface area decreases. This might have an effect on the induction time, and it might affect the growth rate. *Fig* 4.1.2b shows that after 50 hours of hydrate formation, three of the new experiments have the lowest methane consumption. Dep_8 had the highest S_{wi} and have the lowest growth rate *(Fig 4.1.2b.).* Dep_8 experienced an increase in growth rate after approximately 125 hours which is believed to be caused by methane diffusion across the core, thus increasing the water/methane interface over time.

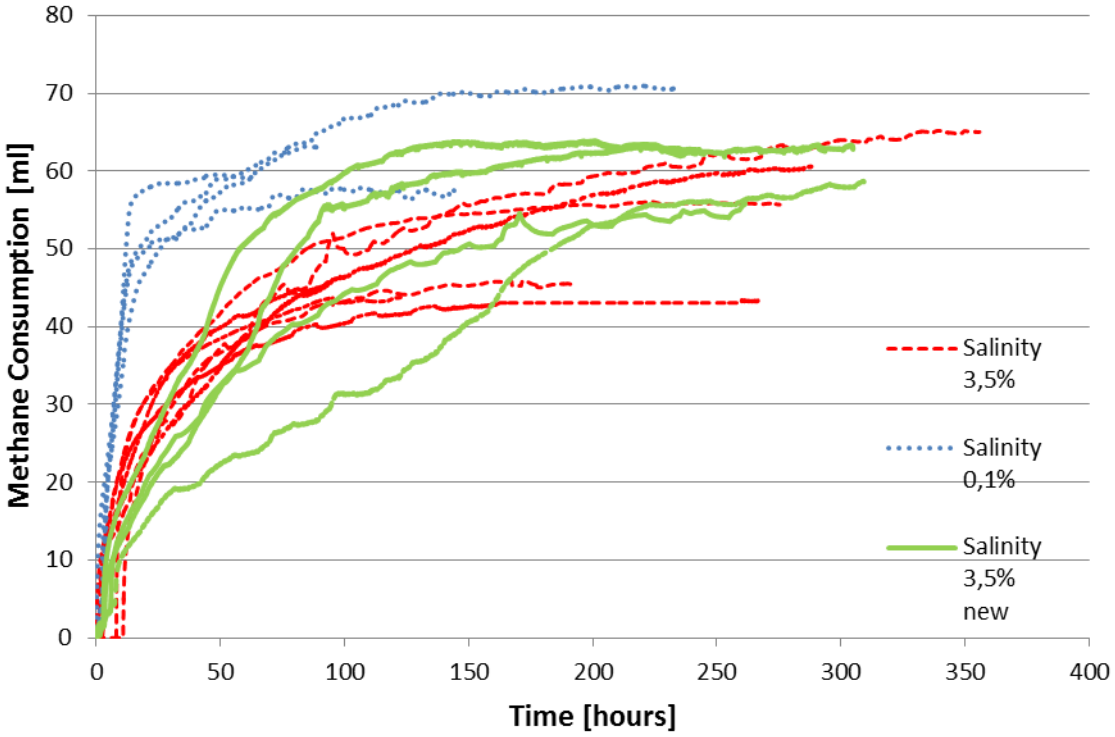

Fig 4.1.2b – Comparison plot of the formation curves from *Fig 4.1.2a* and four of the new experiments. The red and blue lines represents formation curves done with 3.5 and 0.1 weight % respectively and the green line is formation curves from experiments with 3.5% salt concentration conducted recently.

For_2.2 had the highest initial growth rate. This was expected because this was the second hydrate formation done on the same core. The second formation was done 24hours after the hydrates were dissociated from the first formation. When performing two consecutive formations the memory effect causes the second formation to happen faster. The second formation on For_2.2 had an average consumption rate of 3.13 ml/ hour the first 10 hours prior to the induction period (*Fig 4.1.2c)*. As a comparison, HR_58 had 0.87 ml/hour in average during the same time span. HR_58 was used because of its mid-range initial growth rate.

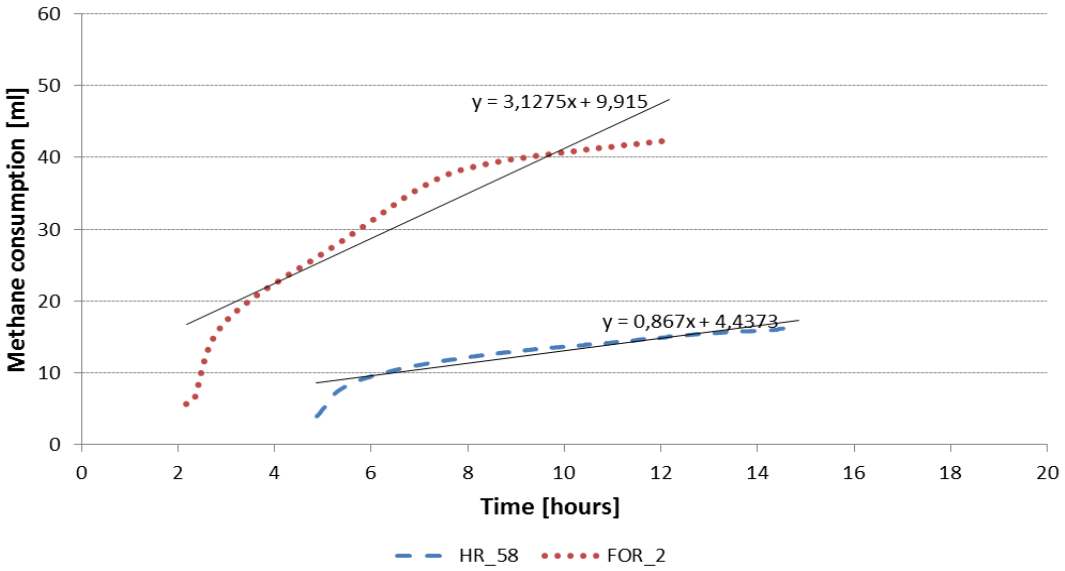

Fig 4.1.2c – Shows the rate of methane consumption the first 10 hours of hydrate formation. This is the second formation done on the For_2.2 core to examine the memory effect.

The resistivity data from the hydrate formation shows a relatively small rate of change in a period after the induction time, which is to expect from the literature (Ren, et al., 2010). Gas hydrates have a low conductivity compared to brine, and as the hydrates forms the tortuosity of the porous media increases. This contributes to an increase in resistivity. The increase in ions in the free water due to hydrate formation lowers the resistivity.

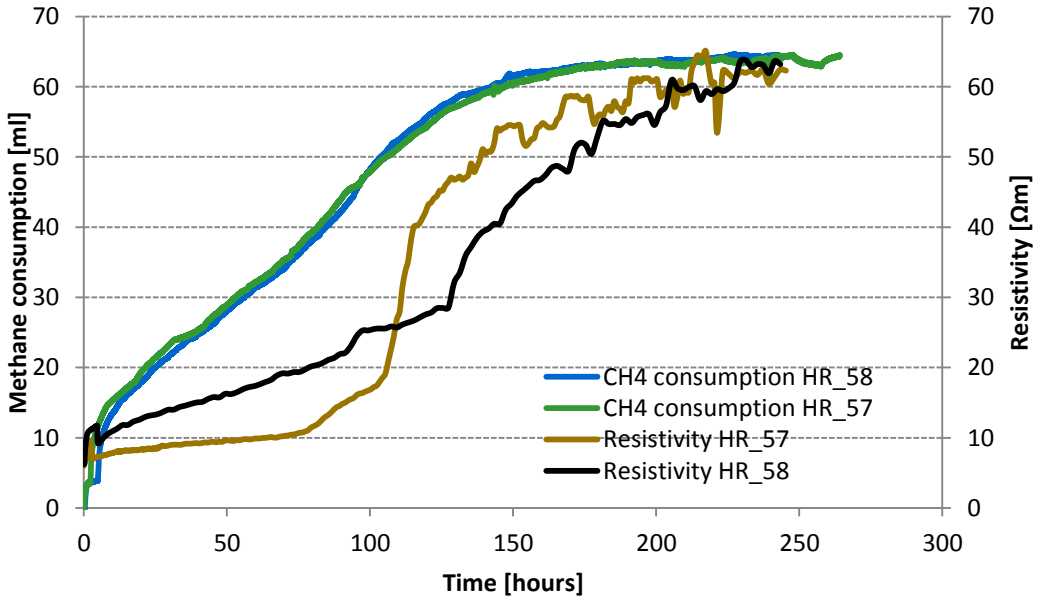

Fig 4.1.2d – Graph over the methane consumption and resistivity during hydrate formation for experiment HR_57 and HR_58. The resistivity increases slowly at low hydrate saturations. Both of the resistivity curves have fluctuations at the end of hydrate formation.

Some literature studies state that the resistivity decreases from the end of the induction period until the hydrate saturation is at 0.20 [frac.] (Ren, et al., 2010). The resistivity in HR_58 has a steady increase when hydrate growth initiates, but the peak value just before the sudden drop at the end of the induction time is not reached before the hydrate saturation is at 0,07 [frac.]. The resistivity increases massively after passing 0.24 [frac.] hydrate saturation, this indicates that the tortuosity

increase dominates the resistivity contribution after this point. The resistivity measurements become more unstable closer to the end of formation, *Fig 4.1.2d*. Small changes in hydrate saturation create relatively big fluctuations in resistivity. An explanation is that hydrates growth in porous media will be heterogeneous and will not reach equilibrium (Sloan & Koh, 2007), this means that there is constant redistribution of hydrate within the core. The hydrates are trying to reach the lowest possible energy state. This redistribution can open and close pathways for the highly concentrated brine (7-13 wt% NaCl) that is left in the core, and therefore make the resistivity fluctuate.

According to Duan et al. the hydrate growth happens on the gas/water interface. On the interface there is abundant of host and guest molecules in addition to good heat transport through the liquid phase. In the pore scale experiment shown below, *Fig 4.1.2e,* this growth process took place in a silicon replica of a Berea sandstone. The water wet grains attracts the water and traps the gas in the middle of the pore. The sandstone used in the core scale experiment is Bentheimer sandstone which is also strongly water wet therefore it is reasonable to believe that the fluid distribution is similar. Another observation is that the hydrate growth is faster where the water that is absorbed on the grains is in contact with the gas bubble. The part of the bubble close to the small grain in the middle covered with hydrate.

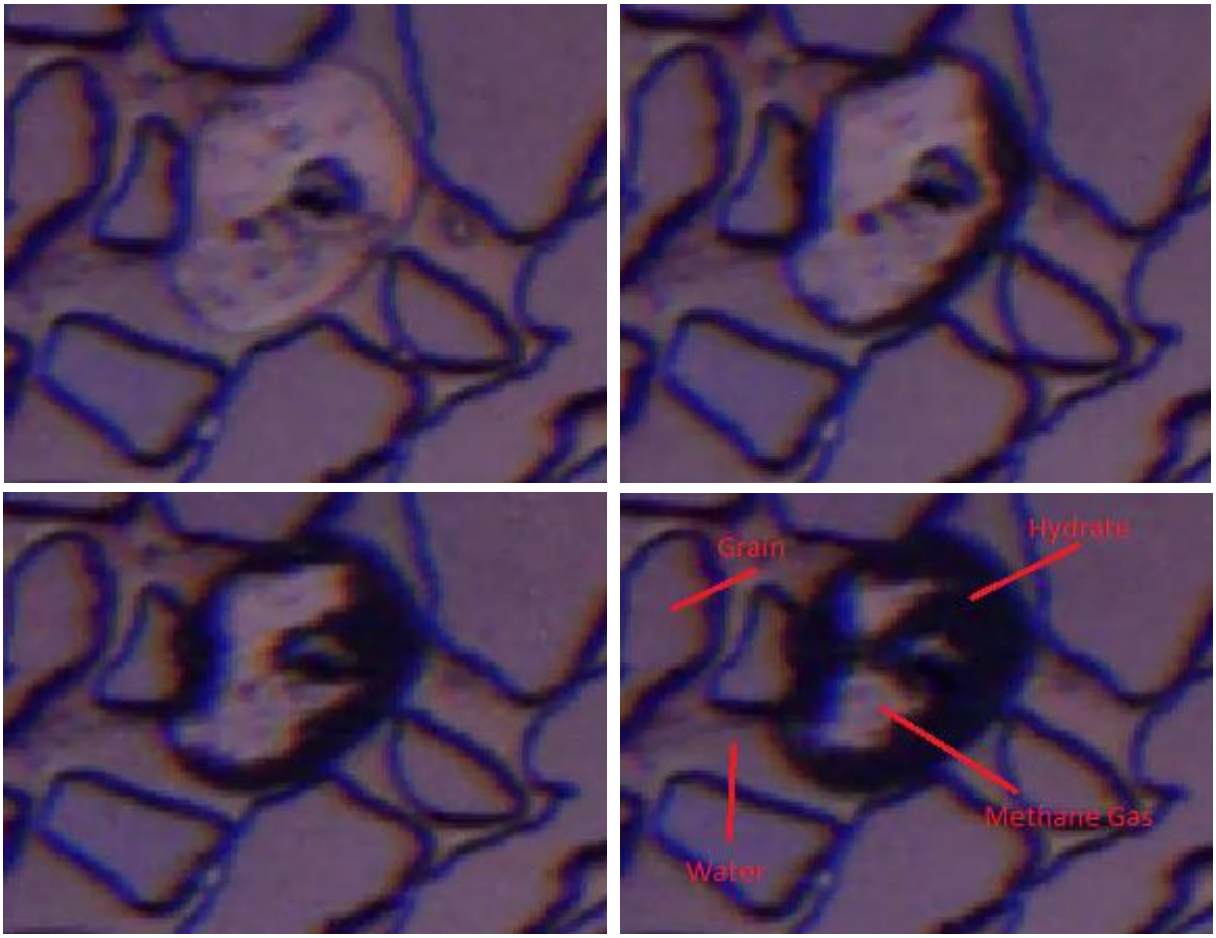

Fig 4.1.2e – Four snapshots from a video of hydrate growth in a micro model. The interval between the snapshots is 30 seconds. The image in the upper left corner shows a bubble of free gas trapped in a big pore, the dark spot in the middle of the bubble is a small piece of grain. Hydrate is growing at the water/gas interface.

4.1.3 Final Saturation

The hydrate saturation was calculated by using the volume log from the injection pump. The volume log states the position of the piston in the pump, the difference in volume before and after formation states how much methane has left the pump. By accounting for the loss due to leakage, the cooling of the core and the effect of water expansion we get the volume of methane that was included in the hydrates.

The range of final hydrate saturation in our experiment is 0.45 – 0.64, where Dep_6 and Dep_9 has the lowest and highest value respectively. Dep_9 also had the lowest formation temperature with 0°C, but no clear trend between final hydrate saturation and temperature was observed. The fact that Dep_6 held 1,5°C during formation helps discard temperature as an important factor in final saturation, within the temperature range of our experiments (0-4°C). Earlier studies done within the hydrate research group suggest that the initial water saturation has an effect on the final hydrate saturation. The 2.order polynomial trend line in Fig 4.1.3a shows an increase in hydrate saturation up to around 0.56 and then decreases. For low initial water saturations there is the obvious restriction in water molecules present in the core. For high initial water saturations the fluid distribution reduces the water/gas surface area, as mentioned in the previous section, and this limits the hydrate formation.

Table 4.1.3 – List over previous experiments done by the hydrate research group that is used in Fig 4.1.3a.

Core_id	Swi [frac.]	Temperature [°C]	Salinity [wt%]	S_{hydrat} [frac.]	Personel
CO2_05	0,52	4	0,1	0,53	Bringedal & Birkedal
CO2_08	0,56	4	3,5	0,52	Bringedal & Birkedal
CO2_09	0,51	4	3,5	0,49	Bringedal & Birkedal
CO2_10	0,33	4	3,5	0,26	Bringedal & Birkedal
CO2_11	0,41	4	3,5	0,39	Bringedal & Birkedal
HR_10	0,65	4	3,5	0,41	Birkedal
HR_38	0,5	4	3,5	0,53	Hauge & Birkedal
HR_39	0,47	4	3,5	0,42	Hauge & Birkedal
HR_46	0,4	4	3,5	0,47	Hauge & Birkedal
HR_47	0,42	4	3,5	0,38	Berge & Hågenvik
HR_48	0,4	4	3,5	0,42	Berge & Hågenvik
HR_49	0,64	4	3,5	0,46	Berge & Hågenvik
HR_50	0,65	4	3,5	0,47	Berge & Hågenvik
HR_51	0,67	4	3,5	0,51	Berge & Hågenvik
HR_52	0,74	4	3,5	0,35	Berge & Hågenvik
HR_53	0,81	4	3,5	0,41	Berge & Hågenvik
HR_56	0,63	4	3,5	0,48	Høyland

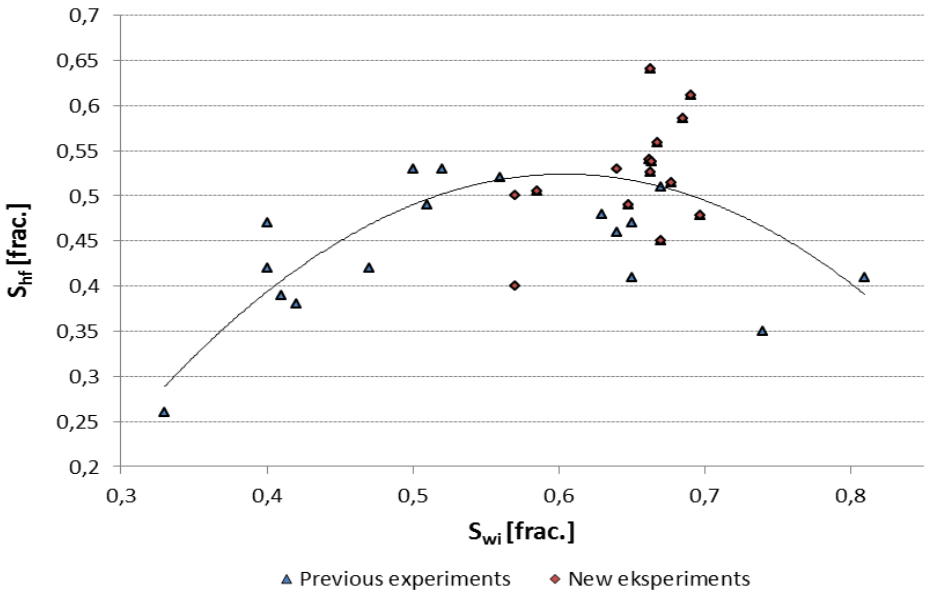

Fig 4.1.3a – Final hydrate saturation plotted against initial water saturation. The red represent experiments conducted by me and Stian Almenningen, and the blue dots is experiments conducted by earlier members in the hydrate research group. The trend line is a second order polynomial of all the experiments.

The final water saturation is an important parameter considering methane production from CO_2/CH_4 exchange. CO2_33 had a S_{wf} = 0.31, which is relatively high. This was a reason why a production scheme involving co-injection of N_2/CO_2 was chosen for methane production, due to challenges involving hydrate plug formation between the excess water and the injected CO_2. *Figure 4.1.3b* shows a trend suggesting S_{wf} is proportional to S_{wi}.

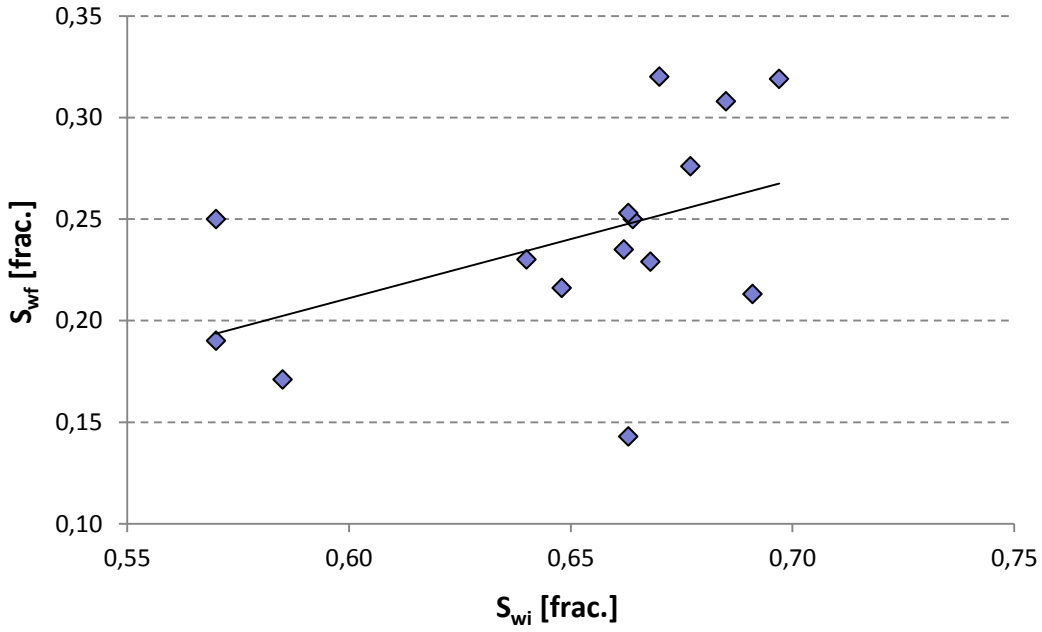

Fig 4.1.3b – Final water saturation plotted against initial water saturation. The trend shows an increase in final saturation with higher initial saturations.

4.2 Depressurization

Methane production by depressurization was executed on 11 cores, important parameters and results are found in *Table 4.2*. The pressure where dissociation was first observed (melting pressure) showed a clear correlation to core temperature, which was expected. The salinity of the excess water post hydrate formation was another parameter expected to affect the melting pressure. These effects of these parameters were also investigated through CSMgem software as described below.

CSMgem was used to get an indication of melting pressures at different temperatures. The CSMgem values in *Table 4.2* were calculated in two different ways; one where the water salinity was kept at 3.5% for all experiments and one where the actual salinity after hydrate formation for each of the experiments was used. The hydration number was set to 5.99 for both of the calculations. The CSMgem calculated dissociation pressures that included the post formation salinities varied from 42.421 to 67.838 bars. The experiments with the lowest calculated post formation salinities were the ones where the observed dissociation pressure best matched the CSMgem pressure. This implies that some of the calculated salinities were too high. The salinities given in *Table 4.2* are calculated from the final fluid and hydrate saturations which are based on the volume of methane consumed in hydrate formation. CSMgem is a hydrate prediction model based on hydrate in bulk. It is uncertain how much the porous media affect the hydrate stability. Hydrate system in porous media with saline formation water is not in equilibrium and will constantly redistribute in order to reach the lowest energy potential (Kvamme, 2014).

Table 4.2 – Results from methane production from depressurization. (1) is the observed melting pressure. The two columns to the right shows the CSMgem calculated dissociation pressure, both of them with the temperatures given in the table. The difference between the two is that (2) is calculated with the actual salinity given in the table and (3)is calculated with 3.5wt% for all.

Core_id	Depressurization temperature [°C]	Salinity [wt%]	Melting Pressure(1) [bar]	CSMgem melt.pres(2) [bar]	CSMgem melt.pres(3) [Bar]
CO2_33	4,0	8,0	42,9	-	-
Dep_6	1,7	7,2	39,6	35,617	42,421
Dep_7	2,8	10,3	37,9	39,823	56,497
Dep_8	2,8	7,4	40,0	39,823	48,037
Dep_9	-0,4	13,5	38,7	28,836	49,189
Dep_10	3,6	8,4	44,3	43,213	55,141
Dep_11	4,2	10,8	42-50	45,961	67,838
Dep_12	4,0	9,8	47,3	45,025	62,396
Dep_13	4,0	9,3	45,2	45,025	60,576
HR_57	4,0	8,9	45,2	45,025	59,191
HR_58	4,0	9,0	47,3	45,025	59,531

4.2.1 Hydrate re-formation

The system is highly sensitive to changes that impact the hydrate stability below the observed melting pressure. Change in either temperature, pressure or salinity may induce rapid hydrate dissociation or re-formation.

During depressurization of dep_12 there was a sudden drop in piston position and a 0.8°C increase in temperature. This occurred at 43.8 bars (*Fig 4.2.1).*This was caused by a temperature increase in the flow loop that cools down the core holder. Dep_12 was conducted in setup B. Setup A and setup B shares the same cooling bath. While dep_12 was depressurizing, a new experiment was initiated in setup A, and when room temperate coolant from setup A entered the shared flow loop, the core temperature in dep_12 increased. This could have been prevented by letting small amounts of room temperate coolant from setup A into the shared flow loop at the time. At 43.8 bars the hydrate had already reached the melting pressure (47.3), and massive dissociation occurred when the temperature increased. When the temperature reestablished at 4°C hydrates started to reform. This is indicated by the shape of the volume curve (1) in *Fig 4.2.1;* it resembles the formation curves in the formation section. Notice the rapid reformation with close to zero induction time due to the "memory effect". The volume stabilized after reformation and depressurization could continue. This temperature induced dissociation can also be observed in *Fig 4.2.2* as a sudden increase in the methane produced during the pressure step at 43.8 bars.

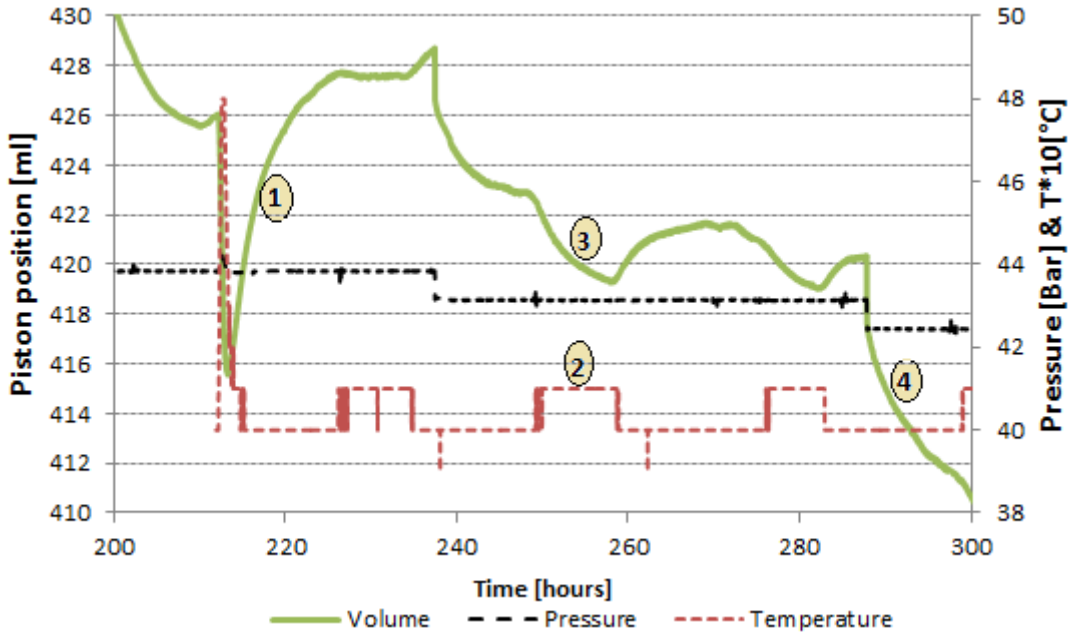

Fig 4.2.1 – shows a 100 hours interval of depressurization of dep_12. (1) Reformation following the massive dissociation. (2) Periodic temperature increase (~0.1°C). (3) Suggested temperature induced dissociation prior to a small reformation. (4) Pressure induced dissociation. The temperature is multiplied by 10 to make the graph orderly. Piston position regulates the volume in the pump, high piston position=low volume available in pump.

There are daily temperature fluctuations in the lab caused by the automatic air condition. These affected the dissociation process. During the temperature fluctuations, the core temperature increased with 0.1°C at the peak (2). As the temperature changes, there is a correlating response in the green volume graph indicated by (3). The piston is retracting due to a pressure increase. A part of

this pressure increase caused to gas expansion in the pump due to the increased temperature, another cause might be temperature induced dissociation. During this depressurization scheme the temperature and pressure conditions balance on the hydrate phase boundary, and a 0.1°C temperature increase might be enough to dissociate some of the hydrate. This is an example of why class 1 hydrate deposits (*section 1.7)* is the most favorable for methane production by pressure induced dissociation. In a class 1 hydrate reservoir the pressure and temperature conditions at the interface between the free gas phase and hydrates coincide with the hydrate stability line. Relatively small amounts of energy are needed to further dissociate the hydrate. This is similar to what is observed in the experiments.

4.2.2 Pressure steps

An interesting result from the pressure step sequence was the low individual recovery from each pressure step (0.7bar) even though the hydrate composition was pure methane and water. The recovery from each step is calculated by Almenningen (2015), were he used the methane density at the given pressure and temperature conditions at each pressure step to convert the volume to moles. The calculations also account for the compaction of water during dissociation.

Twelve pressure steps were conducted on Dep_12 that produced between 3 and 16ml of methane each, the production from each pressure step is shown in *Fig 4.2.2*. This trend was seen in all the depressurization experiment. Those cores that held a lower temperature melted at a lower pressure, but still needed several pressure steps to dissociate 100% of the hydrate. The experiment mentioned in *section 2.4* (Ersland, et al., 2009) was conducted with the same procedure as Dep_12. But all the methane was produced after three pressure steps (39.6, 38.9 and 38.2 bars), and the time spent on each step was 20, 96 and 164 hours. The time spent on each pressure step in Dep_12 varies from 24 to 70 hours, and the number of pressure steps could have been reduced if more time was spend on the early steps. Another difference between the experiments was the salinity. All of the new experiments had an initial salinity of 3.5% while the previous experiment had 0.1%. The higher salinity in the free water face might be the reason for the low methane production for each pressure step. After hydrate formation the salinity in the new experiment ranged from 7.2 to 13.5% (*Table 4.2)* due to NaCl exclusion from the hydrate crystals. When the first hydrate starts to dissociate water molecules are added to the brine and the salinity decreases. This salinity reduction creates a shift in the hydrate stability zone, and the melting pressure is lowered.

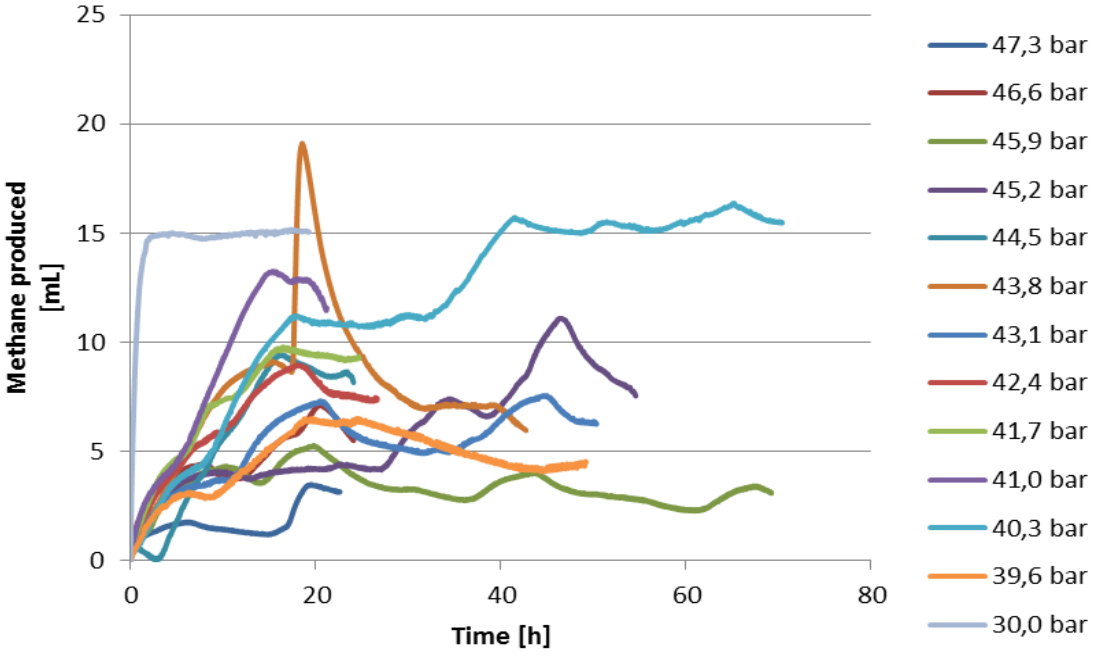

Fig 4.2.2 – Volume of methane produced from the different pressure steps in Dep_12.Modified with permission from (Almenningen, 2015).

Hydrate dissociation is endothermic. This causes heat to be absorbed during dissociation which causes local temperature drops in the porous media. The melting pressure is reduced along with the temperature. This is a partial explanation for the multiple pressure steps needed to produce the methane hydrate, both for the previous and new experiments. Birkedal (2009) proposed that the high hydrate saturation (0.617) in gave a low permeability that lead to the low recovery (9%) from the first pressure step, this is results from the experiment mentioned in *section 2.4*.

4.2.3 Flow test

Due to problems with hydrate plugging after hydrate formation in previous experiments, a flow test conducted on HR_57 prior to the 0.7 bar pressure step scheme. The purpose was to test pressure response across the core, and to identify possible hydrate plugs. The resistivity was measured during the test. The flow test was carried out as described in *section 3.1.8*. As the inlet pressure decreases to 70 bars the first hour the outlet pressure stays at 83 bars. After 20 hours the differential pressure is still at 13 bars. This indicates hydrate plugging. The next pressure step is down to 60 bars. After approximately 2 hours with 23 bars differential pressure the outlet pressure dropped dramatically and pressure response through the core was established. The possible hydrate plug is likely to be found in one of these three places; (1) inside the porous media (2) the channel in the outlet end piece (3) the channel in the inlet end piece. There is estimated 0.25 S_{wf} (*Table 4.1*) which mean that hydrate does not occupy the entire pore space. In addition there is a resistance drop from 63 to 42Ωm during the first pressure step which would not occur if the porous media was plugged. The two previous arguments indicate that the least likely place for the plug is (1). The sudden and rapid drop in outlet pressure after 22 hours supports (2) and (3). The pressure is reduced by increasing the volume in the pump (lowering the piston), when doing this some free water in the core might be drawn in towards the end piece channel. Slight agitation due to the movement in the phases increases the interface between water and gas in the end piece channel thus massive hydrate formation might occur, thus (2) and (3) are the most likely scenarios. The massive initial drop in

resistivity (63-42Ωm) is observed in three different experiments. This is believed to be caused by a redistribution of the phases during the drawback, which results in a more continues water phase with less resistance.

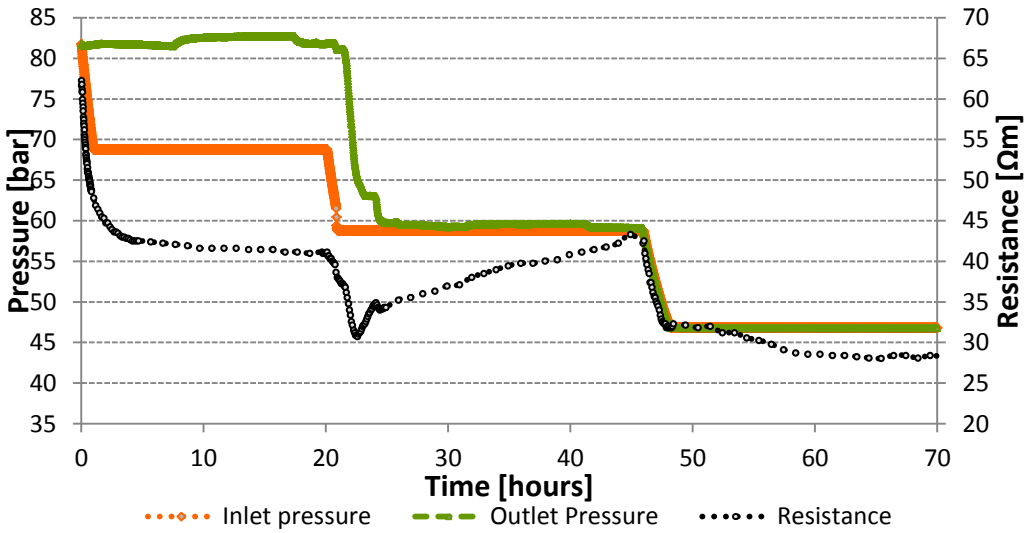

Fig 4.2.3 – First 70 hours of depressurization of Dep_57 with resistivity measurements. The bypass valve was kept closed the first two pressure steps (83-70 bar and 70-60bar) and pressure data was obtained from inlet and outlet transducers.

4.2.4 Limitations of experiment and upscaling

It is important to consider the differences and similarities between field scale and core scale when conducting core scale experiments and interpret the results. An advantage with doing experiments on core samples in a laboratory is the possibility of controlling the different parameters, and in that way be able to identify the impact each parameter have on the system in question. But significant parameters on core scale might be negligible in field scale. The following are some scaling considerations:

The salinity effect on the methane production from the 0.7 pressure step sequence was mentioned in *Section 4.2.2.* This effect was believed to be a significant factor in the low gas production from the individual pressure step due to the high salinity in the residual water, post formation. In a hydrate reservoir the salinity of the formation water will most likely equal the salinity in the water surrounding the reservoir, due to molecular diffusion over a long period of time. Even if the permeability of the reservoir is small due to high S_h, the amount of time between formation and production will make the salinities equalize.

Heat absorption from the endothermic hydrate dissociation process can be a challenge. In the setup used in this thesis, the surroundings consisted of a liquid flow loop, thus no change in the temperature due to dissociation was observed, but local temperature gradients might exist locally in the core without affecting the temperature sensor. Heat absorption is more significant in the field, it is a major challenge. If the hydrate dissociation rate is high relative to the local heat transport in the reservoir, the formation water might freeze and hydrate re-formation might occur. The Messoyakha field in Siberia supposedly produces methane from a class 1 hydrate deposit, and reports that frequent freezing and re-formation is a challenge (Grace, et al., 2008).

Water production is a challenge connected to gas production from hydrate dissociation. Water is released during the hydrate dissociation, and is produced along with the gas. Water was observed in the tubing and in the pump cylinder after each depressurization experiment. The Bentheimer sandstone used in the experiments is consolidated and relatively rigid, therefore little sand was found in the production water. In some hydrate reservoirs the hydrates are contributing to the geomechanical stability of the formation, and by dissociation the hydrate the formation may lose its geomechanical integrity. The Mallik production test, mentioned in *section 2.1.3,* experienced a lot of sand production due to the unconsolidated nature of the reservoir (Grace, et al., 2008). Conventional hydrocarbon production also experience problems with sand production, but usually not that severe due to the reservoir fluids low contribution to the formation strength compared to the contribution of gas hydrates. The loss of geomechanical integrity may also cause landslides.

4.3 Experiment CO2_33; the effects of CO_2

CO2_33 were the only experiment with successful methane production from CO_2/CH_4 exchange. The experiment consists of hydrate formation, exchange and depressurization and lasted for 73 days. This section will contain results and discussion of the exchange and depressurization part of the experiment. Each section will start by presenting important results followed by a more detailed investigation of the experiment.

4.3.1 CO_2/CH_4 exchange

An estimated methane recovery of 0.25 from hydrate was obtained after injecting 3.6 PV of a fluid mix consisting of CO_2 (40%) and N_2 (60%) through 2.5-8.8 hour intervals (*Table 3.1.6)*. 47.6 hours of effective injection time was spent on the flushing sequence. The methane recovered from hydrate together with the total methane recovery and cumulative methane produced is shown in *Fig 4.3.1a.*

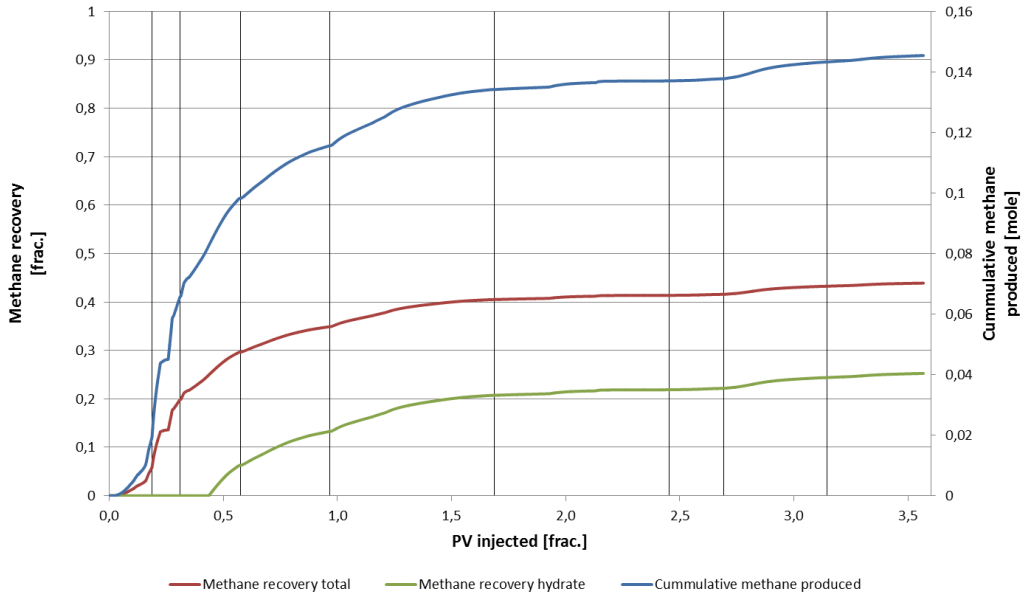

Fig 4.3.1a – Methane recovery and cumulative methane produced from the CO_2/N_2 fluid mix flush sequence in CO2_33 plotted against pore volume injected. The vertical lines in the graph separates each flush in the sequence. Modified with permission from (Almenningen, 2015).

After hydrate formation S_{hf} and S_{wf} were 0.59 and 0.31 respectively. In a similar experiment (HR_56 (Høyland, 2014)) the saturation were S_{hf}=0.50 and S_{wf}=0.24. No pure N_2 flush was performed prior to

the CO_2/N_2 injection. This resulted in a rapid increase in differential pressure (ΔP) indicating hydrate plugging. Pure N_2 was then injected in order to obtain flow. For approximately 500 hours the N_2 pump was connected to the core while being in the constant pressure setting before flow through the core was established. To prevent hydrate plugging in CO2_33 a 5 hour N_2 flush was performed prior to CO_2/N_2 injection (*Fig 4.3.1b)*.

Fig 4.3.1b shows an increase in ΔP during the 5ml/hour N_2 injection. There is a sudden increase in ΔP approximately 0.5 hours before injection stops. This is due to the outlet pressure exceeds 85 bars, and some of the gas passes the BPR and the outlet pressure decreases, hence increasing ΔP. After stopping the pump and isolating the core there is a rapid decrease in ΔP which indicates that the permeability is sufficient to initiate the CO_2/N_2 sequence. Even though a N_2 flush has been done there is still a chance of CO_2 hydrate forming near the end piece-channel and plug the system.

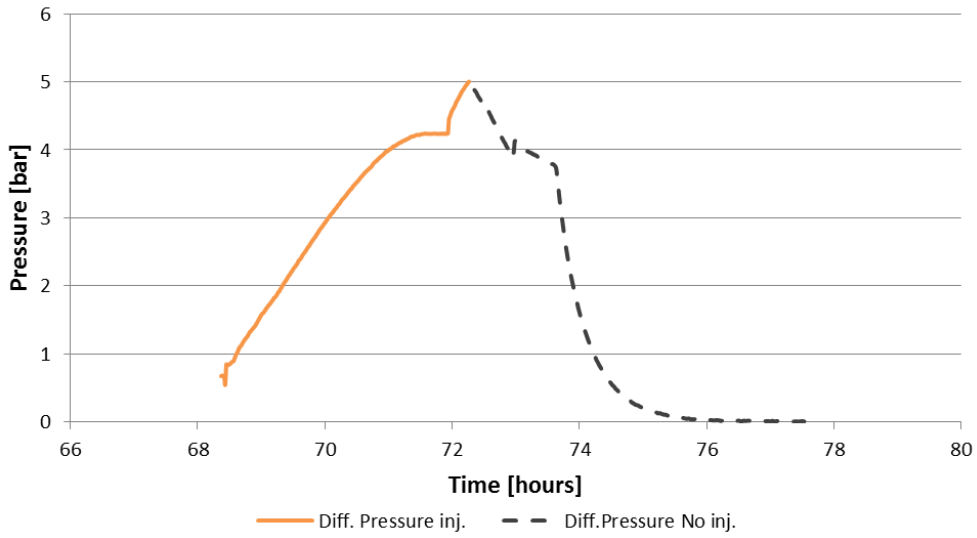

Fig 4.3.1b – Differential pressure between inlet and outlet transducer during the N_2 flush prior to the CO_2/N_2-sequence. Solid orange line represents differential pressure during injection, black dashed line is diff pressure when stopping the injection and isolating the core.

There is a high methane fraction (0.6-0.9) in the production during the first two CO_2/N_2 flushes (*Fig4.3.1c)*. This is probably the free methane left in the core and tubing being produced and not methane released from hydrate. The free methane produced is the sum of the excess gas in the core post hydrate formation (0.062 moles) and the methane residing in the tubing between the core and the inlet and outlet valves (0.020 moles). After the 3rd flush the N_2 fraction is at 0.60, thus the production of N_2 is equal to the injection. The CO_2 fraction in the gas production does not reach the injected fraction (0.4) until the 6th flush (approximately 2 PV injected). It is expected that CO_2 will be trapped due to solid -exchange with CH_4-hydrate, but the amount is uncertain. Some of the CO_2 might also form hydrate with the free water phase.

While the N_2 fraction remains relatively stable around 0.6 and the CO_2 and CH_4 curve are more dependent on each other (*Fig 4.3.1c)*.When the CH_4 fraction increases the CO_2 fraction decreases and the other way around. This dependence is an indication of CO_2/CH_4 exchange. Notice the sudden increase in the methane fraction shortly after (1-2 hours) commencing a new flush. This

phenomenon is believed to be caused by CO_2 diffusion during the non-injection period between each flush. More CH_4-hydrate is exposed to CO_2 due to diffusion, and the CH_4 that is excluded in the exchange process will be produced during the next flush. After injecting 2.5 PV *Fig 4.3.1c* shows an increase in the methane fraction by approximately 0.14 during flush 7 and 8. An inverse response is observed from the CO_2 fraction which indicates CO_2/CH_4- exchange.

Park et al (2008) observed methane recoveries between 64 -95% in CO_2/CH_4 –exchange done with bulk hydrates. One of the production mechanisms in the bulk experiments was believed to be that N_2 molecules competed with CH_4 molecules for the small cavity in structure one hydrates. There is little indication of any N_2 being trapped in hydrate in CO2_33. The mass balance of N_2 in CO2_33 shows an equal amount of gas injected as produced during the first 7 flush injections. After the 7th flush there is a drop in the mass produced, this is assumed to be a leak in the production line. *Fig 4.3.1c* shows an increase in N_2 after the 7th flush interval which supports the leak assumption and supports the claim that little or no N_2 is trapped by hydrate formation.

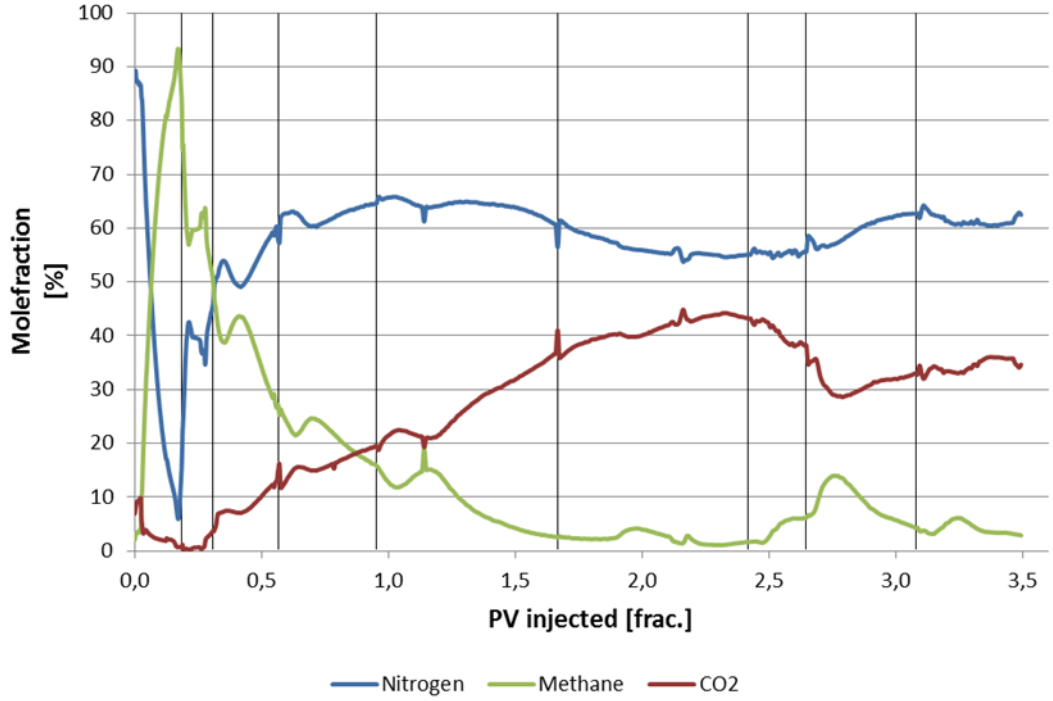

Fig 4.3.1c – Composition of the gas production from CO2_33. The mole fraction of each gas is read by the GC and plottet against PV injected. The vertical lines represent the different flushes in the production sequence. Modified with permission from (Almenningen, 2015).

Experiments done with a split core with a spacer in the middle have a methane recovery of 50-85% of the methane in hydrate (Graue, et al., 2008). The spacer in the middle of the core increases the contact area between the CO_2 and CH_4 hydrate which may contribute to a better recovery than observed in CO2_33. In a whole core, which was used in CO2_33, the molecular diffusion is believed to be more significant than in a fractured core, in respect to the exchange process. Indicating that methane production and CO_2 sequestration is more time dependent in a whole core. The flush sequence was stopped during the 10th flush due to GC problems. At this point there was still some methane being produced (*Fig 4.3.1c).* A higher methane recovery would most likely be obtained if the experiment were not concluded. Another factor that leads to an underestimation of the methane recovery is the leak in the setup that presumably occurred after the 7th flash. CO_2 is not likely to

occupy the small cages in the hydrate structure do the size ratio, thus the theoretical maximum of methane recovery by exchange is 75% (Ersland, 2008).

Due to the leak the estimated CO_2 sequestration in hydrates were not based on the mass balance. The estimated CO_2 sequestration in hydrates is 0.26 moles. This estimate is based on the assumption that each methane molecule that was produced from hydrate was replaced by a CO_2 molecule, indicating no dissociation of methane hydrate or N_2/CH_4 exchange during the flush-sequence. In the ignic Sikumi field trial there was estimated 48 Mscf of CO_2 left if the reservoir as a free phases, trapped in hydrate or dissolved in water. The estimated total methane production was 860 Mscf (Schoderbek, et al., 2012). This gives a molar ratio between the CO_2 left in formation/ total CH_4 produced of ~0.06 which indicate a large amount of methane gas being produced from other processes than CO_2 exchange (initial free methane, methane hydrate dissociation, N_2 exchange).

4.3.2 Depressurization of CO2_33

There hydrate mix of both CO_2 and CH_4 inside the sandstone core sample after the CO_2/N_2 flush sequence were done. In addition there were probably free fluid phases of water, methane, nitrogen and carbon dioxide. The depressurization method used is described in *section 3.1.7* and is the same procedure that is used in the pure methane hydrate depressurizations. Because of the heterogeneous nature of the hydrate system in CO2_33 it is expected that hydrate will melt in a wider range of pressures than for the pure methane experiments.

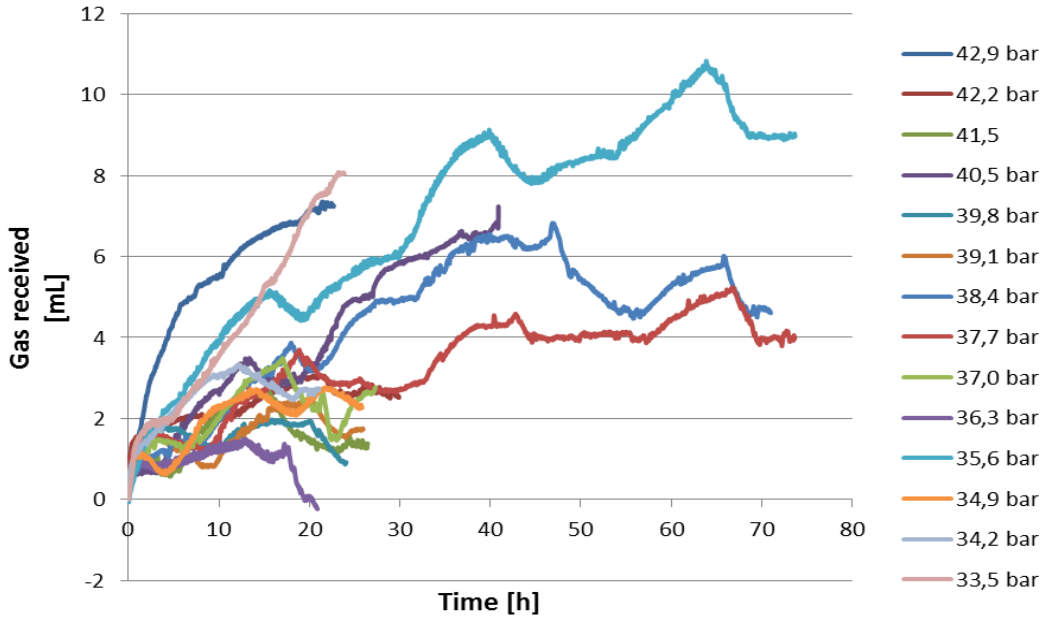

Fig 4.3.2a – Volume of gas produced from each pressure step in CO2_33. 14 pressure steps are plotted. Figure modified with permission of (Almenningen, 2015).

Hydrate dissociation was observed at 42.9 bars. Methane hydrate has a higher dissociation pressure than CO_2-hydrate thus pure methane hydrate is assumed to dissociate first. The mole fraction of CH_4 and CO_2 was calculated by using CSMgem software for each pressure step where dissociation occurred. *Fig4.3.2b* shows the amount of hydrate of each mole fraction. The last pressure step is from 33.5-21.7 bars and approximately 35% of the hydrate dissociated during this step. Prior to the

last pressure step it was assumed that most of the hydrate was dissociated. In retrospect the series of 0.7bar pressure steps could have continued to lower pressures before executing the final pressure step. This would give a better indication of the CO_2 occupancy in hydrate in the 0.5-1 range (*Fig4.3.2b).*

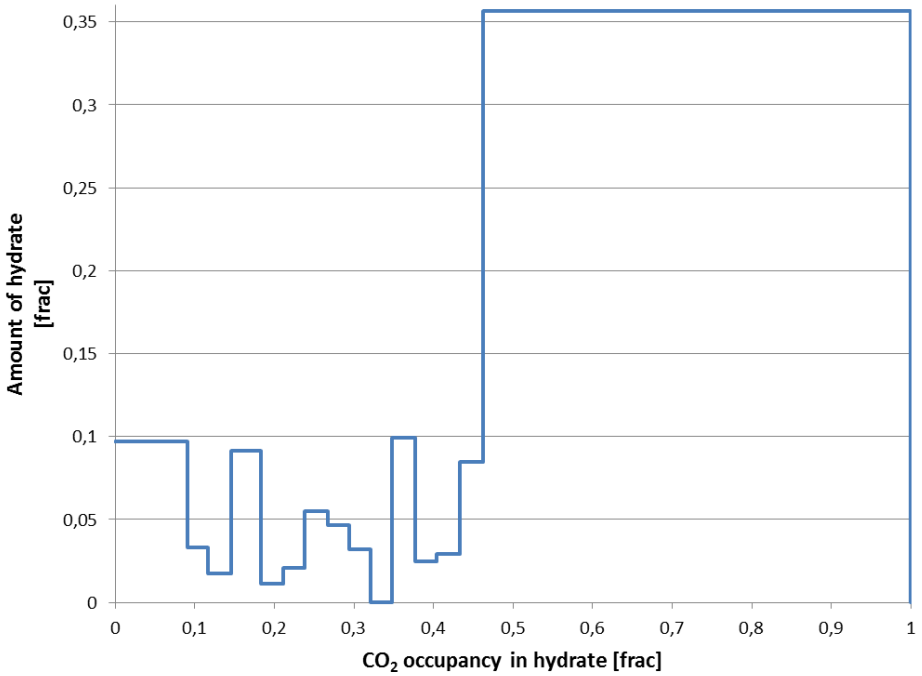

Fig 4.3.2b – Suggested hydrate composition of CO2_33 prior to depressurization. The mole fraction of CO_2 and CH_4 is calculated for each pressure step with CSMgem software. The mixed density for each hydrate composition together with the volume of gas released for each pressure step is used to find the amount of hydrate for each CO_2/CH_4 composition. Modified with permission from (Almenningen, 2015).

There are several deviations between the conditions used in the calculations and the actual conditions: (1)CSMgem is a hydrate saturation model based on hydrates in bulk. (2) The salinity is set to 3.5% for all pressure steps, but in reality the salinity will be higher at the first step and then decrease as the hydrates dissociate. (3) The nitrogen present in the core is not part of the CSMgem calculations. According to CSMgem the dissociating pressure for pure CO_2-hydrate is 24.35bar with 3.5% salinity in the formation water at 4°C. Because of the relatively high starting point (33.5 bars) on the final pressure step it is difficult to determine at what pressure the dissociation ceased. Previous in-house experiment, HR_48 (Hågenvik, 2013), displays hydrate dissociation down to 26.9 bars. 31.7 bars was the first pressure step where dissociation was observed in HR_48 and no N_2 had been injected in the core. Another in-house experiment, HR_49 (Hågenvik, 2013), used co-injection of N_2/CO_2 during the exchange process prior to the depressurization. Hydrate dissociation was first observed at 34.5 bars in HR_49 and the dissociation continued down to 30.3 bars (*Fig 4.3.2c)*.

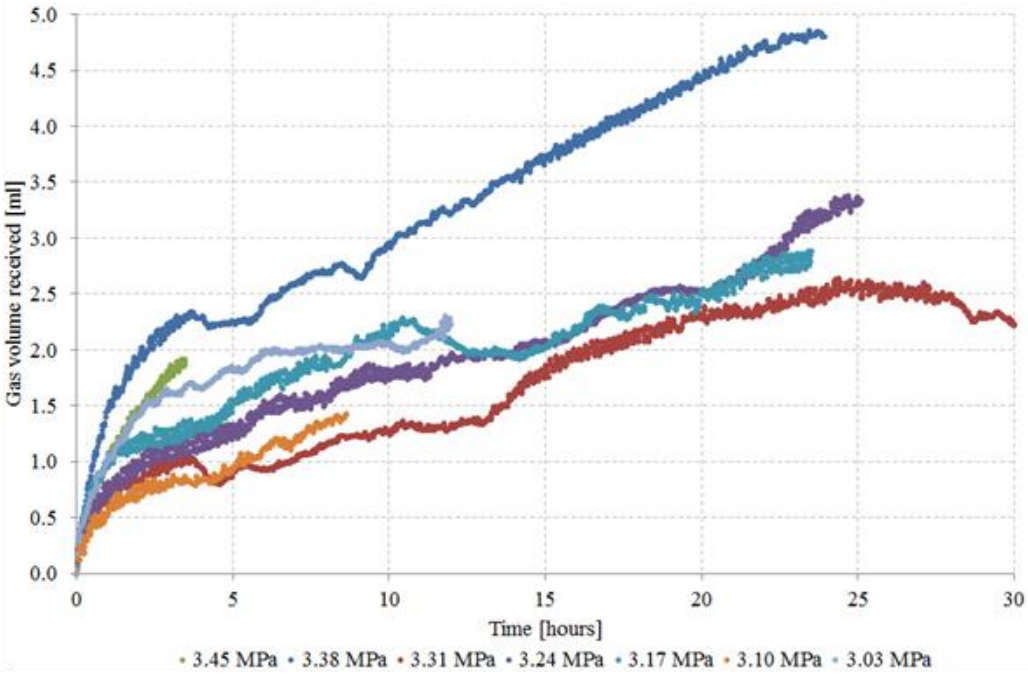

Fig 4.3.2c – Volume of gas produced from each pressure step in HR_49 (Hågenvik, 2013).

4.3.3 Limitations of experiment and upscaling

Ignik Sikumi is the only production field test where CO_2/CH_4 exchange has been tested; therefore there is little experience in how the production scheme influences the hydrate reservoir and the surroundings. The exchange process in itself is believed to be a solid state conversion, thus avoiding the challenges connected to hydrate dissociation. There are other considerations when dealing with CO_2/CH_4 exchange:

The heat released during the exothermic exchange process may create local temperature gradients, and thermally induce hydrate dissociation, thus increase the amount of released methane. In a hydrate reservoir where the heat transport might be limited by massive hydrate deposits, it reasonable that the heat release can cause dissociation if the pressure and temperature conditions is sufficiently close to the hydrate stability line. No dissociation was observed in CO2_33 during the exchange process. The reason is probably because of the efficient heat transport in the core setup, combined with the relative high pressure and low temperature conditions.

The pore volume (PV) injected is an important parameter in a commercial perspective. 3.6 PV of CO_2/N_2 mixture was injected in CO2_33 over a 10 day period. In an actual hydrate reservoir this would probably not be a viable option, due to the cost and the high injection rate needed (depending on the size of the reservoir).

4.4 MRI

A series of tests was conducted at the new hydrate lab on Statoil Sandsli together with the hydrate research group. The lab is in a development process and the tests were conducted to assist in the calibration of the MR-apparatus. The first test was to image one phase flow through Bentheimer Sandstone with 100% water saturation. Heavy water (^2H_2O) was injected into the core to establish flow. The difference in gyromagnetic ratio between the two hydrogen isotopes causes a difference in the MRI signal from H_2O and ^2H_2O: This made it possible to follow the propagation of the heavy water through the core. The other test was to image cyclopentane hydrate dissociation within a Bentheimer Sandstone core. To slow down the dissociation process the core was covered in bubble wrap post hydrate formation. The dissociation occurred faster than expected, and by the time the first image was captured, the most of the hydrate had already dissociated. Fig 4.4 below show an image from 1 and 3 hours after the core was placed in the MR-apparatus. There is slightly more signal from the right image (3h) as indicated by the brighter core, this is probably due to some hydrates still left in the middle of the core after 1 hour.

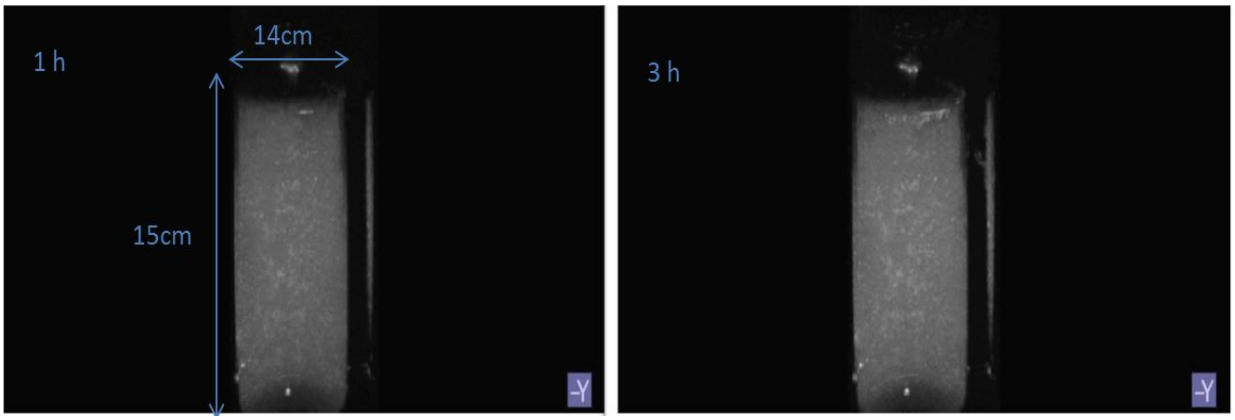

Fig 4.4 – MR images of a Bentheimer sandstones core initially saturated with cyclopentane-hydrate from 1 and 3 hours after initiating temperature induced dissociation.

4.5 Uncertainties

Some degree of uncertainty is always present in experimental work. These uncertainties may include human error, damaged equipment and uncertainty in the equipment itself. The equipment used in these experiments is relatively precise and did not dominate the degree of uncertainty. When dealing with gas under pressure it is difficult to avoid any leakage in valves and fitting and this was probably the biggest contributor to the uncertainty. The assumptions made during the calculations will also be listed in this section.

4.5.1 Leakage

After pressurizing the core prior to hydrate formation the pump volume is monitored for at least 24 hours to check for leakage. Leakage rates in the range of 0.000 – 0.130 ml/hour were estimated for the hydrate formation and depressurization. The leakage rate for CO2_33 was estimated to 0.015 ml/ hour during formation and depressurization, but when executing the flush-sequence the leakage rate was higher and less predictable. Section 4.3.1 mentions a leak after the 7th flush. This was most likely a leak between the GC and MFM which resulted in an underestimation of the methane recovery.

4.5.2 Equipment uncertainty

Even though the uncertainties given by the manufacturer are relatively low (*Table 4.4.2)* greater error may occur if the equipment is damaged. In the initial experiments there was some trouble with the temperature readings. The output temperature was higher than the core temperature. The thermometers in question were tested after the experiments ended and the offset temperatures were recorded. The GC broke down after CO2_33 was finished. The reason was probably water production from the core during the flush-sequence. During the 10th flush the GC stopped to record any CO_2 which is why the flush-sequence was ended.

Table 4.5.2 – Uncertainties of the equipment given by the manufacturer.

Equipment	Measurement	Uncertainty	Unit
Slide caliper	Length	± 0.01	cm
GF-3000 Digital Balance	Weight	± 0.02	g
ST Stigma 500	Flow	± 0.1	%
	Pressure	± 0.1	%
HH506RA Thermometer	Temperature	± 0.1	°C

4.5.4 Calculating uncertainties

The uncertainties accompanying the initial conditions such as bulk volume, initial water saturation and salinity where calculated with the following equations:

In these calculations the equipment uncertainty for each measurement is used as δx_i :

$$\delta R = \sqrt{\left(\frac{\partial R}{\partial x_1}\delta x_1\right)^2 + \left(\frac{\partial R}{\partial x_2}\delta x_2\right)^2 + \cdots + \left(\frac{\partial R}{\partial x_n}\delta x_n\right)^2} \quad (4.5.4a)$$

For a sum of multiple variables, R = ax + by + cz, the uncertainty is given:

$$\delta R = \sqrt{(a\delta x)^2 + (b\delta y)^2 + (c\delta z)^2} \quad (4.5.4b)$$

For a product of multiple variables, $R = a \cdot x^n \cdot y^m \cdot z^k$, the uncertainty is given:

$$\delta R = R\sqrt{\left(n\frac{\delta x}{x}\right)^2 + \left(m\frac{\delta y}{y}\right)^2 + \left(k\frac{\delta z}{z}\right)^2} \quad (4.5.4c)$$

In the equations above δR is the calculated uncertainty and δx_i is the equipment ucertainty. n,m and k is the potens of the variable. R is the calculated value. x,y z is the measured values. The uncertainties in *Table 4.4.4* is calculated with the equipment uncertainties (*Table 4.4.2)* and the equations above. Other uncertainties related to the initial conditions have been neglected. For instance loss of formation water during core weighing due to evaporation causes an underestimation of S_{wi}. The matrix density is used together with V_b to calculate V_p and the porosity, but this uncertainty is also neglected.

Table 4.5.4 – Calculated values for the initial conditions in CO2_33 with uncertainties. The matrix density is used to find V_p, but this uncertainty is neglected.

Parameter	Calculated value	Unit	Uncertainty	Unit
S_{wi}	0.69	frac.	±0.01	frac.
V_b	298	ml	±1	ml
V_p	70	ml	±1	ml
Salinity	3.50	weight %	±0.01	%

4.5.5 Gas volume uncertainty

The volume of gas injected/retracted from the pump is an important parameter. The volume of methane is key when calculating hydrate saturation. Final salinity and excess water saturation are derived from the hydrate saturation. The daily temperature fluctuations in the lab are ±1°C. This results in a core temperature fluctuation of ± 0.2°C which does not affect the gas volume significantly. The pump cylinder is not isolated and the temperature fluctuations in the room cause the volume of gas in the pump to vary with ±0.7ml at 83bar by the ideal gas law.

4.5.6 Phase distribution uncertainty

The CO_2 is liquid in the injection pump, but when reaching the core it mixes with other gases which shift the liquid/gas phase boundary towards higher pressures (Jung, et al., 2010). The CO_2 is also cooled down from ~22 to 4°C in the core; this effect decreases the phase boundary pressure. It is uncertain if the CO_2 was in liquid phase or gas phase. If the CO_2 is liquid inside the core it may act as a drying agent as stated in *section 1.2.*This might reduce the excess water saturation. Liquid CO_2 is a more effective heat and mass conductor than the gaseous phase which can affect the hydrate saturation.

Chapter 5 – Conclusions and Future Work

Conclusions

Methane formation was conducted successfully in 15 different Bentheimer sandstone cores with initial water saturations in the range of 0.57-0.70 and a salinity of 3.5wt% NaCl. The results from the experiments have been added to the in-house database.

No correlation was found between induction time and temperature in the interval investigated (0-4°C). A trend showing increasing induction time with increasing initial water saturation was obtained. Comparison of current and previous experiments indicates that salinity of the formation-water have a more significant impact on the hydrate growth rate than on the final hydrate saturation.

During the depressurization induced dissociation a higher amount of pressure steps (~12) were needed to produce all the methane than observed in previous similar experiments (~3). The salinity in the free water phase increases during formation and decreases during dissociation, thus constantly shifting the hydrate boundary line which leads to low gas production in each pressure step.

Gas production was observed in fourteen 0.7bar pressure steps and one 11.8bar pressure step during the depressurization of CO2_33. The highly heterogeneous nature of the hydrate mix between CO_2 and CH_4 with additional free nitrogen present and high salinity water caused a large interval of dissociation pressures.

An estimated methane recovery of 0.25 was obtained from CH_4/CO_2 – exchange by co-injection of 40%CO_2 and 60%N_2 in a flush-sequence of 9 successful flushes resulting in an effective injection time of 47.6 hours.

The mix of CO_2 (0.4) and N_2(0.6) was a success in maintaining injectivity throughout the flush-sequence. After with a five hours flush of pure nitrogen, the co-injection was initiated and no plugging was observed.

Hydrate growth was observed at pore scale. It was apparent that hydrate growth occurred on the liquid/gas interface between water and methane. Video and still images were obtained from the formation process.

Future work

More experimental work on CO_2/CH_4 exchange as a production scheme is needed. Due to problem with the GC there was only one successful experiment conducted using this scheme during this theses. The initial purpose was to examine a porous media with relatively high excess water saturation while injecting CO_2/N_2 in order to obtain methane production, CO_2 sequestration and prevent additional hydrate CO_2 formation. Setup C with the extra flow path can be modified further by adding an alternative flow path to the outlet end piece as well, and therefore be able to check for possible hydrate plugs in both inlet and outlet.

The setup at the hydrate lab at Statoil Sandsli needs further development. In order to image the hydrate formation process a temperature control unit need to be integrated in the MRI-setup. A pressure cell also needs to be integrated to investigate CH_4 hydrate by MRI.

Nomenclature

S_{wi}	initial water saturation
S_{wf}	final water saturation
S_{hf}	final hydrate saturation
S_h	hydrate saturation
S_g	gas saturation
ΔG	change in Gibbs free energy
X_i	mole fraction of component i
ΔP	differential pressure
t	time
t_i	induction time
R	uncertainty
R_t	total resistivity
r	resistance
V_b	bulk volume
V_p	pore volume
T	temperature
f	fugacity
K*	hydrate growth constant
K_r	reaction rate constant
K_d	mass transfer coefficient
n	mole
n_i^{mi}	n_i is the number of edges in face type "i" and m_i is the number of faces with n_i edges
A	surface area
V_H	hydrate volume
V_{CH4}^H	volume of methane consumed during hydrate formation
ρ	density
μ	dipole moment
y	gyromagnetic ratio
w_0	precession frequency
M	magnetization
B_0	static magnetic field
m	mass
M_w	molar weight

Abbreviations

frac.	fraction
GC	Gas chromotograph
kcal	Kilo calories
kJ	Kilo Joules
MFM	Mass flow meter
MRI	Magnetic resonance imaging
Mtoe	Million tons of oil equivalent
NGH	Natural gas hydrates
NMR	Nuclear magnetic resonance
SI	Structure 1
sII	Structure 2
sH	Structure H
Tscf	Trillion standard cubic feet
wt%	Weight percent

Bibliography

Almenningen, S., 2015. *An experimental study of methane hydrates in sandstone cores,* Bergen: University of Bergen.

Birkedal, K. A., 2009. *Hydrate Formation and CH4 Production from Natural Gas Hydrates,* Bergen: University of Bergen.

Birkedal, K. A., 2013. *Empirical and Numerical Evaluation of Mechanisms in Gas Production from CH4 - Hydrates.* Bergen: University of Bergen.

Bosewell, R. & Collett, T., 2006. The Gas Hydrate Resource Pyramid. *Fire in the Ice*, pp. 1-2.

Chang, R., 2006. *General Chemistry.* 4th ed. New York: The Mcgraw-Hill Companies.

Ch'ng, L. C., n.d. *USC Dornsife.* [Online]
Available at: https://dornsife.usc.edu/lee-chng/what-we-do/
[Accessed 10 December 2014].

Collett, T., 2002. Energy Resource Potential of Natural Gas Hydrates. *AAPG Bulletin,* Issue 86.

Dirdal, E., Arulanantham, C., Sefidroodi, H. & Kelland, M., 2012. Can cyclopentane hydrate formation be used to rank the performance of kinetic hydrate inhibitors?. *Chemical Engineering Science,* 82(12), pp. 177-184.

Duan, Z., Møller, N., Greenberg, J. & Weare, H., 1992. The prediction of methane solubility in natural waters to high ionic strength from 0 to 250°C and from 0 to 1600 bar. *Geochimica et Cosmochimica acta,* Volume 56, pp. 1451-1460.

Energy, U. D. o., 2014. *eia.* [Online]
Available at: http://www.eia.gov/tools/faqs/faq.cfm?id=73&t=11
[Accessed 15 march 2015].

Ersland, G., 2008. Magnetic Resonance Imaging. In: *Studies of flow mechanisms and hydrate phase transitions in fractured rocks.* Bergen: University of Bergen, pp. 23-27.

Ersland, G., Birkedal, K. A. & Graue, A., 2009. *MRI Characterization of Hydrate Growth pattern and Production Scenarios in Sandstone.* Moscow, Gubkin Russian State University of oil and Gas.

Grace, J. et al., 2008. *Energy From Gas Hydrates: Assessing The opportunities and Challanges For Canada,* Ottawa: Council of Canadian Academies.

Graue, A. et al., 2008. MRI Visualization of Spontaneous Methane Production From Hydrates in Sandstone Core Plugs When Exposed to CO2. *SPE,* pp. 146-147.

Grover, T., Moridis, G. & Holditch, S., 2008. *Analysis of reservoir performance of Messoyakha Gas hydrate Field.* Vancouver, ISOPE.

Hester, K. & Brewer, P., 2009. Clathrate Hydrates in Nature. *Annual Reviews.*

Hornbrook, J. W., Castanier, L. M. & Pettit, P. A., 1991. *Observation of Foam/Oil Interactions in a New High-Resolution Micromodel.* Dallas, SPE.

Hossainpour, R., 2013. *Catalysts for Enhanced CO2-CH4 Exchange in Natural Gas Hydrates,* Bergen: University of Bergen.

Husebø, J., 2008. *Monitoring Depressurization and CO2-CH4 Exchange Production Scenarios for Natural Gas Hydrates:.* Bergen: University of Bergen..

HWU, 2013. *What are Gas Hydrates. from HERIOT WATT INSTITUTE OF PETROLEUM ENGINEERING.* [Online]
Available at: http://www.pet.hw.ac.uk/research/hydrate/hydrates_what.cfm?hy=what

Høyland, M. D., 2014. *Measurements and visualization of hydrate growth in porous media,* Bergen: UiB.

Hågenvik, C., 2013. *CO2 Injection in Hydrate Bearing Sandstone with Excess Water,* Bergen: UiB.

International Energy Agency, 2014. *Key World Energy Statistics,* Paris: IEA.

Jha, K. & Bansal, G., 2012. *Will Gas Hydrate Lying on Oceanic Floors in India Solve Its Energy Problem? A Futuristic Approach.* Copenhagen, SPE.

JOGMEC, 2014. *Road to Offshore Gas Production Test - From Malik to Nankai Trough.* Texas, Offshore Technology Conference.

Jung, J., Espinoza, D. & Santamarina, J., 2010. Properties and phenomena relevant to CH4 and CO2 replacement in hydrate bearing sediments. *Journal of Geophysical Research,* Volume 115, pp. 1-16.

Karanjkar, P., Lee, J. & Morris, J., 2011. Calorimetric investigation of cyclopentane hydrate formation in an emulsion. *Chemical Engineering Science.*

Klauda, J. & Sandler, S., 2005. Global Distribution of Methane Hydrate in Ocean Sediment. *Energy and fuels,* 2(19), pp. 459-470.

Kleinberg, R. et al., 2003. Deep sea NMR: Methane hydrate growth habit in porous media and its relationship to hydraulic permeability, Deposit accumulation, and submarine slope stability. *Journal of Geophysical Research,* Volume 108.

Kvamme, B., 2014. *Lecture note.* Bergen: s.n.

Kvenvolden, K. A., 1988. Methane Hydrate - A Major Reservoir of Carbon in the Shallow Geosphere. *Chemical Geologi*, 7 july, pp. 41 - 51.

Lien, J., 2004. NMR-Logging. In: *Ptek211-Grunnleggende Reservoarfysikk.* Bergen: Universitetet i Bergen, pp. 55-76.

Lien, J., 2004. *PTEK211 Grunnleggende reservoarfysikk (kjerneanalyse og logging).* Bergen: Universitetet i Bergen.

Moridis, G. et al., 2010. *Challenges, Uncertainties, and Issues Facing Gas Production From Gas-Hydrate Deposits. Spe Reservoir Evaluation & Engineering.* Pittsburgh, SPE.

Park, Y. et al., 2008. *SWAPPING CARBON DIOXIDE FOR COMPLEX GAS HYDRATE STRUCTURES.* Vancouver, Proceedings of the 6th International Conference on Gas Hydrates.

Rangel-German, E. & Kovscek, A., 2006. A micromodel investigation of two-phase matrix-fracture transfer mechanisms. *Water Resources Research,* Volume 42.

Ren, S., Liu, Y., Liu, Y. & Zhang, W., 2010. Acoustic velocity and eletrical resistance of hydrate bearing sediments. *Journal of Petroleum Science and Engineering,* Volume 70, pp. 52-56.

Ruppel, C., 2011. *Methane Hydrates and the Future of Natural Gas,* s.l.: U.S Geological Survey.

Schoderbek, D. et al., 2012. *North Slope Hydrate Fieldtrial: co2/ch4 Exchange.* Texas, Artic technology conference.

Sloan, E. D., 1998. *Clathrate Hydrates of Natural Gases.* 2nd ed. New York: Marcel Decker, Inc..

Sloan, E. D. & Koh, C., 2007. *Clathrate Hydrates of Natural Gases.* Third Edition ed. s.l.:Taylor & Francis.

Stillinger, F. H., 1980. Water Revisited. *Science*, 25 july.

Wischnewski, B., n.d. *Peace Software.* [Online]
Available at: http://www.peacesoftware.de/einigewerte/co2_e.html
[Accessed 22 may 2015].

Yamamoto, S. K., Terao, Y., Fujii, T. & Terumichi, I., 2014. *Operational overview of the first offshore production test of methane hydrates in the Eastern Nankai Trough.* Texas, Offshore Technology Conference.